Marine and Petroleum Geology 112 (2020) 104074

Contents lists available at ScienceDirect

Marine and Petroleum Geology

journal homepage: www.elsevier.com/locate/marpetgeo

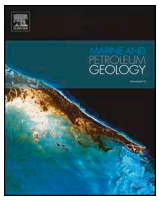

Research paper

Structural controls on shallow fluid flow and associated pockmark fields in the East Breaks area, northern Gulf of Mexico

Chantelle Roelofse[a,*], Tiago M. Alves[a], Joana Gafeira[b]

[a] 3D Seismic Lab, School of Earth and Ocean Sciences, Cardiff University, CF10 3AT, United Kingdom
[b] British Geological Survey, The Lyell Centre, Research Avenue South, Edinburgh, EH14 4AP, United Kingdom

ARTICLE INFO

Keywords:
Focused fluid flow
Pockmarks
Mud volcanoes
Spatial distribution
Gulf of Mexico salt basin

ABSTRACT

Three-dimensional (3D) seismic data, combined with semi-automated mapping in ArcGIS, were used to analyse the morphology and distribution of 720 pockmarks and 62 mud volcanoes in the northern Gulf of Mexico. The relationship amongst salt bodies, faults and the distribution of pockmarks and mud volcanoes stresses the significance of these structures in focusing fluid flow on continental margins. The pockmarks were classified according to their structural setting and depth of source, and later correlated with seep data from the Bureau of Ocean Energy Management (BOEM). Key findings include: a) half of the pockmarks are located within faults rooted on the top of salt diapirs, whilst 96% of the pockmarks are associated with salt diapirs – emphasising the importance of salt and crestal faults in focusing fluid flow to the sea floor; b) diffusion flow through the salt minibasins is clear due to the presence of soft amplitude anomalies (indicating fluids) and pockmarks located far from salt or faults; c) oil and gas are actively leaking to the sea floor; d) a higher density of fluid flow features are found in areas with steeper minibasin dips and greater catchment areas. While no clear correlation is evident between the morphological attributes and depth of source, the shallow plumbing system is dominated by pockmarks, whereas mud volcanoes are sourced from the deeper parts of the salt minibasins. In summary, this study uses a novel approach to analyse the plumbing system in a salt-rich basin based on the recognition of surface fluid flow features. The importance of characterising the fluid flow features and associated structures to reduce risk and uncertainty is stressed in terms of both shallow gas hazards and hydrocarbon leakage from deeper reservoirs.

1. Introduction

Pockmarks are fluid migration features first discovered by King and MacLean (1970) as shallow depressions on the sea floor, generated as overpressured fluids expelled to the surface. This typically violent eruption propels sediment into the water column, sediment which is then transported away by bottom currents. Pockmarks have since been widely imaged by multibeam, echosounders, sidescan sonar and seismic data, and are indicative of focused fluid flow to the surface (eg Hovland and Judd, 1988). Pockmarks are usually connected to a source region at depth by fluid pipes of variable lengths and widths. These are narrow, vertical features which cross-cut seismic reflections, effectively high- or low-amplitude seismic anomalies with columnar geometry in three dimensions (Cartwright and Santamarina, 2015; Løseth et al., 2011).

In the last two decades, much research has focused on the formation of pockmarks and pipes, as well as their spatial relationship with underlying structures. These include buried turbiditic channels, salt diapirs and polygonal faults (Gay et al., 2003; Andresen et al., 2008; Maia et al., 2016). Pockmarks comprise engineering challenges and hazards for seafloor infrastructure and exploration drilling (Judd and Hovland, 2007). Many studied pockmark fields have been found to be related to shallow gas, particularly when this gas is produced by methane hydrates that are dissociated by pressure or temperature changes (Judd and Hovland, 1992; Rollet et al., 2009). Evidence for shallow gas in seismic data may include acoustic haze or dimming, enhanced seismic reflections (or bright spots), and phase reversals, to name a few (Judd and Hovland, 1992). In contrast, mud volcanoes are positive fluid escape features on the sea floor that chiefly comprise mud and other sediments. They periodically or continuously vent liquid mud, water and hydrocarbon products, forming in thick sedimentary basins where significant overpressures build at depth – often due to rapid sedimentary loading and hydrocarbon generation (Mazzini, 2009). These phenomena result in density inversion and upward mobilization of deep mudstones and accompanying fluids (Brown, 1990; Milkov, 2000; Judd

* Corresponding author.
E-mail addresses: roelofsec@cardiff.ac.uk (C. Roelofse), alvest@cardiff.ac.uk (T.M. Alves), jdlg@bgs.ac.uk (J. Gafeira).

https://doi.org/10.1016/j.marpetgeo.2019.104074
Received 21 June 2019; Received in revised form 2 October 2019; Accepted 4 October 2019
Available online 07 October 2019

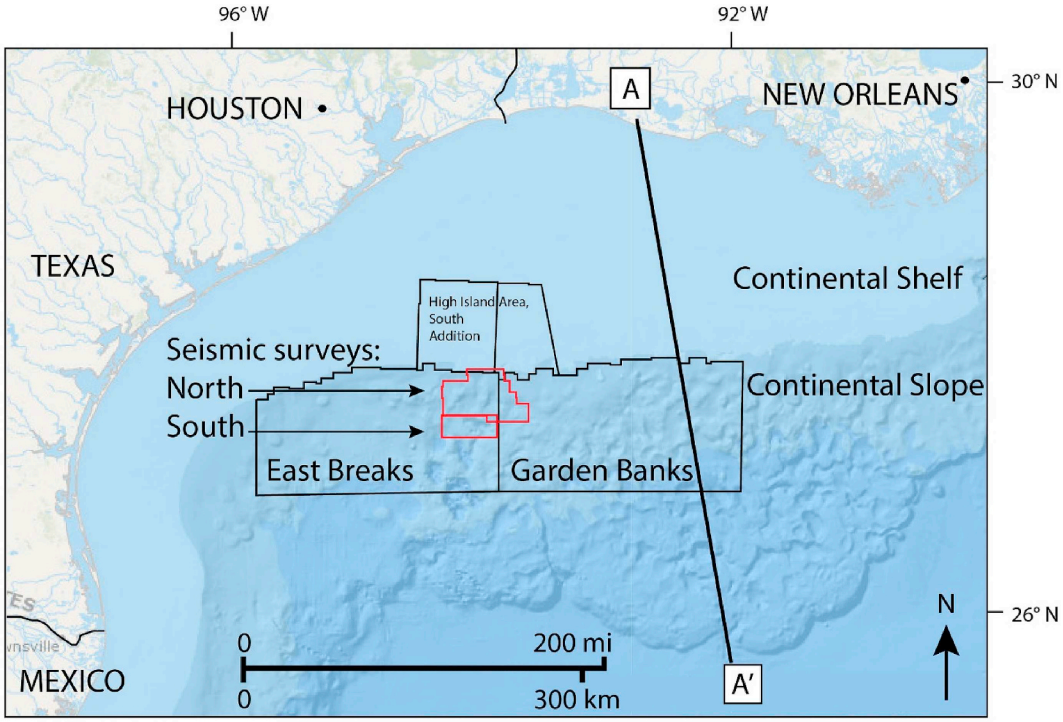

Fig. 1. Location map of study area. The two 3D seismic surveys are outlined in red in the north-eastern corner of East Breaks, northern Gulf of Mexico. The regional line A-A′ is shown in Fig. 2. (For interpretation of the references to colour in this figure legend, the reader is referred to the Web version of this article.)

and Hovland, 2007). Therefore, mud volcanoes are important indicators of deep plumbing systems in a sedimentary basin.

Enhancements in the resolution and processing of 3D seismic data have allowed for more detailed analyses of submarine features. For instance, Andresen et al. (2011) and Ho et al. (2018) correlated both seafloor and buried pockmarks with deep hydrocarbon sources offshore Angola, suggesting active plumbing systems and tertiary migration in the Lower Congo Basin. The Northern (US) Gulf of Mexico is a mature, hydrocarbon-rich basin with over 53,000 wells drilled along the continental margin into deeper waters (400–7000 ft) (Kaiser, 2018). Oil slicks and gas plumes have been detected in the study area (East Breaks, Gulf of Mexico) amongst fields of pockmarks and mud volcanoes, indicating an active hydrocarbon plumbing system. However, the study area contains few wells and no producing fields have been discovered to date (Fig. 1). As shown by Xia and Wilkinson (2017), seal failure and leakage from reservoirs (tertiary migration) can lead to losses in the economic value of hydrocarbon prospects; these economic risks need to be fully accounted for in successful hydrocarbon field cases, thereby highlighting the importance of identifying indicators of hydrocarbon leakage. Against such a background, the aims of the paper are as follows:

- Characterise the morphology and distribution of pockmarks and mud volcanoes and relate to the structures at depth;
- Describe the plumbing system of East Breaks and discuss the implications for hydrocarbon trapping and leakage in this case study for exploration in salt basins;
- Conclude whether the interpreted fluid flow features can be used as a predictive tool for the depth of hydrocarbon source intervals.

2. Geological framework

2.1. Mesozoic evolution of the northwest Gulf of Mexico

The northwest Gulf of Mexico is dominated by systematic, thermally driven subsidence overprinted by eustatic base-level changes (Watts, 1982; Galloway, 1989). Its generalised stratigraphy is summarised in Figs. 2 and 3. In the Late Triassic, the North American plate rifted from Pangaea to form a series of grabens and half-grabens filled with continental red beds and volcanic rocks, known collectively as the Eagle Mills Formation (Salvador, 1987). Deposition of sedimentary units in a coastal plain to shoreface environment followed during an Early Jurassic transgression (Hudec et al., 2013). By the Middle Jurassic, initial connection to the Pacific Ocean formed a semi-restricted basin in which the Louann salt was deposited (Fig. 4a). Hudec et al. (2013) estimated that 3–4 km of salt was deposited in as little as 2 Ma, assuming similar depositional rates to thick salt basins in the Mediterranean Sea (Krijgsman et al., 1999) and southeast Brazil (Pietzsch et al., 2018).

Further rifting and extension of the continental crust led to continental break up, formation of oceanic crust and seafloor spreading during the Late Jurassic, separating the Louann salt basin from the southern Campeche (Mexican) salt basin (Fig. 4c) (Bird et al., 2005). Post-rifting thermal subsidence resulted in deepening of the basin as the connection with the North Atlantic Ocean was being established. This resulted in widespread deposition of organic rich, deep-marine shales during the Latest Jurassic (Tithonian) (Hood et al., 2002), generating one of the major source rock intervals in the Gulf of Mexico. Seafloor spreading ended by the earliest Cretaceous (c. 140 Ma), marking the start of the passive-margin phase. This passive-margin structure remained inherent to the Gulf of Mexico basin until the present day.

In contrast to the Jurassic, slow rates of clastic sediment influx generated a largely carbonate depositional system during the Cretaceous (Galloway, 1989).

2.2. Cenozoic evolution and salt tectonics

During the Paleogene, the Laramide inversion caused uplift of the Sierra Madre Occidental in Mexico and renewed uplift of the Rocky Mountains in North America, resulting in the reintroduction of large volumes of clastic sediment in the Gulf of Mexico via the Rio Grande and Houston Delta Systems (Galloway et al., 2000). The deposition of thick (8–14 km) deep-marine units in the northwest Gulf of Mexico

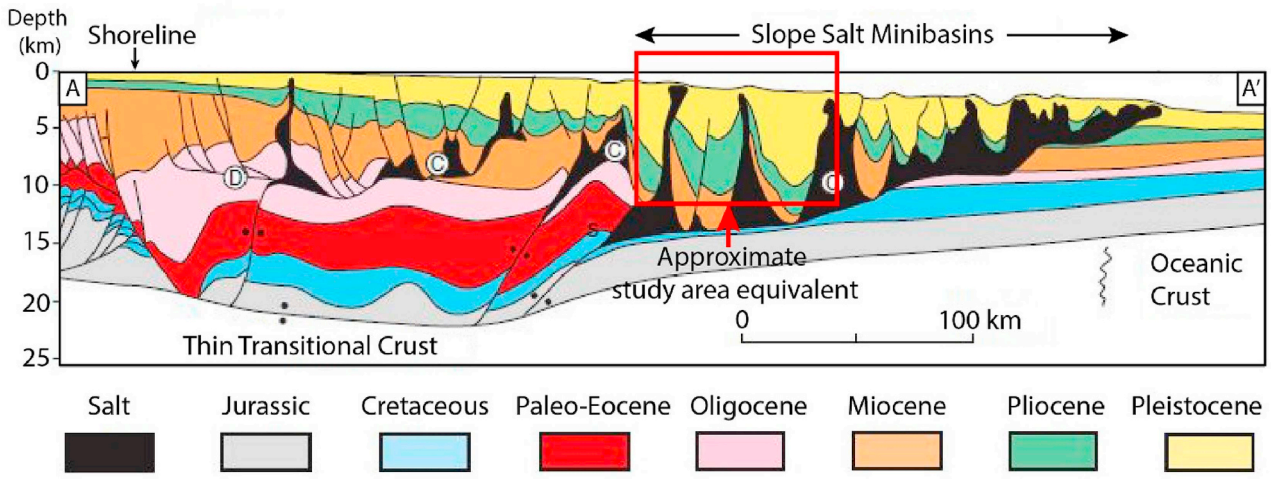

Fig. 2. Regional seismic line through the northern Gulf of Mexico. The red box indicates the approximate location of the study area, projected. Location given in Fig. 1. Modified from Galloway (2008). (For interpretation of the references to colour in this figure legend, the reader is referred to the Web version of this article.)

caused flexural loading, initiating gravitational tectonics and salt mobility (Galloway, 1989). This led to the development of large-scale structures including salt canopies, allocthonous salt sheets, salt diapirs and salt welds (e.g. McBride et al., 1998; Rowan et al., 1999). These structures deformed the palaeo-seafloor bathymetry and continue to do so at present, spatially controlling the deposition of younger sediments (Fig. 5). Simultaneously, deep burial of the Jurassic (Tithonian) source rock resulted in hydrocarbon generation (Hood et al., 2002).

During the Cenozoic, the continental shelf of the Gulf of Mexico prograded ~290 km southwards and produced up to 18 genetic sequences (Feng, 1995). These sequences consist of deep-water turbidites confined within canyons, salt minibasins, or deposited as submarine fans on the basin floor. The turbidites are capped by condensed deep marine hemipelagic mud, biogenic oozes and reworked transgressive/retrogressive slope facies (Galloway et al., 2000).

3. Methodology

3.1. Interpreted database

Two 3D seismic-reflection surveys migrated in time were interpreted in the East Breaks region, on the upper slope of the northern Gulf of Mexico (Fig. 1). The northern survey B-32-91-TX covers an area of 2031 km^2 and was acquired in 1991 by Calibre Seismic Company. The survey was processed in zero-phase, SEG positive standard polarity such that an increase in acoustic impedance with depth manifests as a peak and is coloured black, whilst a trough is coloured red (Fig. 6). Bin spacing is 20 × 25 m and the vertical sampling rate is 4 ms two-way-time (TWT). The dominant frequency is 50 Hz and, using equations defined by Badley (1985), the tuning thickness ($\lambda/4$) at the sea floor is 8 m, for a vertical limit of detectability ($\lambda/30$) of 1 m.

The southern dataset was acquired in 1989 by Shell Offshore Inc., covers an area of 835 km^2 and was processed in zero-phase, SEG negative standard polarity – as this is the opposite to the northern dataset, the colour bar was flipped so that the datasets visually match. A trough is coloured black and represents an increase in acoustic impedance with depth. Bin spacing is decimated to 100 × 100 ft with a vertical sample rate of 4 ms TWT. The dominant frequency is 35 Hz; tuning thickness at the sea floor is 11 m and the vertical limit of detectability ($\lambda/30$) is 1.3 m. Water depth ranges from 85 m–1395 m, deepening to the south (Fig. 5).

No well logs were available in the study area. Nevertheless, detailed stratigraphic descriptions are provided by Beaubouef and Friedmann (2000), whose study area overlaps with the westernmost part of this survey (Fig. 5).

The Bureau of Ocean Energy Management (BOEM) recently published a regional bathymetric map of the northern Gulf of Mexico and interpreted several seafloor anomalies such as pockmarks, oil slicks and seismic amplitude anomalies. These anomalies are available in the form of Geographic Information System (GIS) shapefiles (Kramer and Shedd, 2017); the anomalies were imported into Petrel and compared with fluid flow features and deeper structures identified in seismic data. The methodology adopted in this work is summarised in Fig. 7.

3.2. Seismic interpretation

Two seismic horizons were mapped, the sea floor and 'Horizon 1', which is the deepest and most continuous reflector that could be traced across the minibasins (Fig. 6). The seismic variance attribute was used to highlight irregularities such as faults, pockmarks, and salt bodies. Variance is a measure of laterally adjacent seismic waveform similarity; similar traces are mapped as low variance values, while discontinuities have high variance values (Brown, 2011). The seismic volume attribute 'Consistent Dip' was applied, from which Dip and Dip Azimuth seismic volumes were created. These attributes were extracted at the sea floor and Horizon 1 in the salt minibasins, so as to determine the areas of greater dip and – opposite to dip azimuth – the migration pathways from minibasins to supra-salt strata. Seismic artefacts such as acquisition footprints have been accounted for during quality control to ensure that interpretations represented true geology (Marfurt and Alves, 2014).

3.3. ArcGIS semi-automated mapping and characterisation

In a first stage, the mapped seafloor surface from the 3D seismic data was converted from the time to depth domain and exported from Petrel into ArcGIS 10.7. An ArcGIS-based Toolbox developed by the British Geological Survey, the BGS Seafloor Mapping Toolbox (Gafeira et al., 2012; Gafeira et al., 2018), was used to semi-automatically map the confined depressions (pockmarks) on the sea floor and extract any relevant morphological attributes. These include vertical relief, area, width, length, width:length ratios, which were summarised in a table of attributes in ArcGIS. These characteristics were used to compare the pockmarks and correlate them with different structures and trends. Manual quality control was required due to the highly faulted and irregular nature of the sea floor in the study area – some seafloor depressions automatically mapped do not correspond to true 'pockmarks', whilst other clearly visible pockmarks were missed by the Seafloor

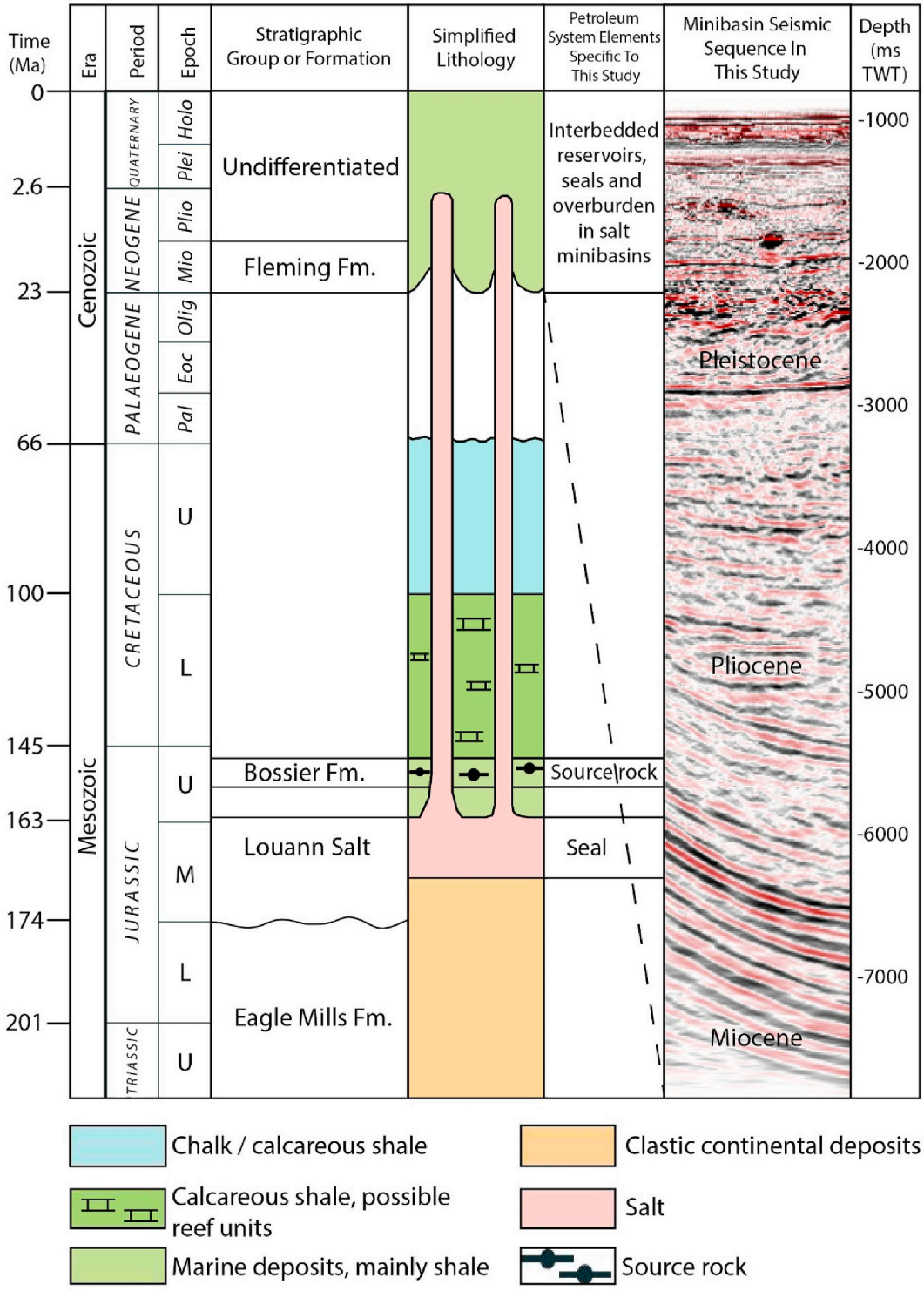

Fig. 3. Mesozoic-Cenozoic stratigraphic section of the East Breaks area of the northern Gulf of Mexico coastal plain, with petroleum system elements specific to this study. Modified from Hackley and Ewing (2010) and Mello and Karner (1996).

Mapping Toolbox. The latter were mapped manually. The number of pockmarks which require manual editing should never exceed 10% of the total number of pockmarks delineated by the Toolbox – otherwise, it may be wise to redefine the input parameters and re-run the latter (Gafeira et al., 2012). The selected input parameters are shown in Table 1.

Although the Seafloor Mapping Toolbox can also trace positive features, the mud volcanoes were manually mapped as the Toolbox processing time was deemed too long, in the order of hours, compared to less than an hour to map them manually. In addition, many positive structures such as fault scarps were found to be incorrectly mapped as mud volcanoes. A subset of the Toolbox called 'Short Description Tool' was run for the mud volcanoes to calculate their morphological attributes, namely width and vertical relief (Figs. 12, 19 and 20).

Seismic resolution is a key consideration when interpreting fluid flow features such as pockmarks and pipes. The resolution is very high near the sea floor (~8 m tuning thickness, ~1 m detectability), though in other basins in the world ROV/multibeam data have revealed

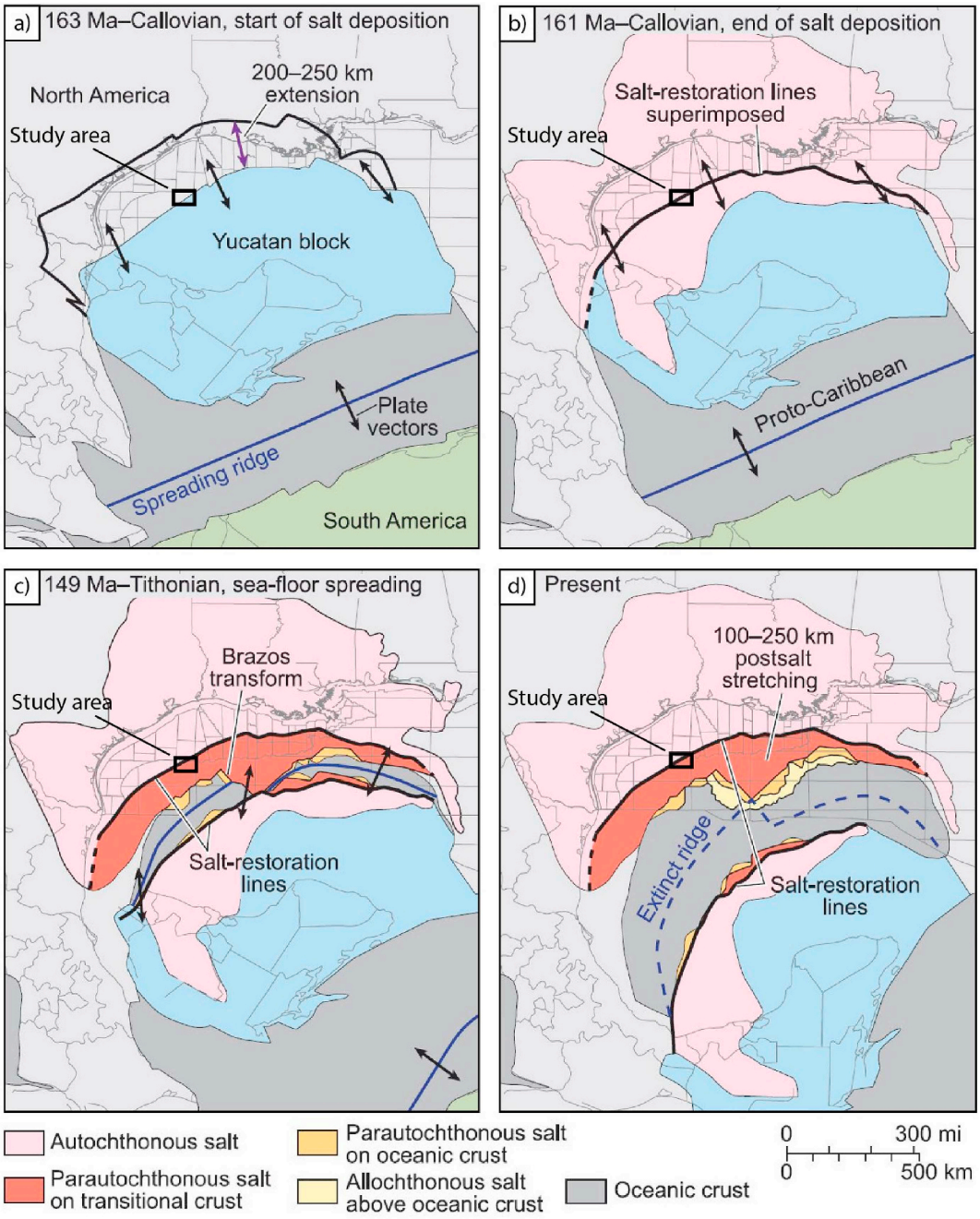

Fig. 4. Palaeogeographic reconstruction of the Gulf of Mexico basin; a) 163 Ma – Callovian, start of salt deposition; b) 161 Ma – Callovian, end of salt deposition; c) 149 Ma – Tithonian, seafloor spreading; d) Present day, with study area labelled. Modified from Hudec et al. (2013).

pockmark fields at sub-metre scale (Hasiotis et al., 1996; Moss et al., 2012). It is possible that much smaller pockmarks do exist in the study area as these are not always resolved in seismic data. Also, the Seafloor Mapping Toolbox identified pockmarks that were not mapped by the BOEM, confirming how easy it is to miss pockmarks.

3.4. Structural relationship and depth prediction

The pockmark and mud volcano shapefiles were exported into Petrel® to identify the underlying structures in the seismic profiles and manually estimate the depth of source for each fluid-flow feature to the interpreted structure, in milliseconds two-way time (TWT). The depth of source of pockmarks was estimated to the nearest 50 ms TWT, whilst the depth of source of the mud volcanoes was estimated to the nearest 100 ms TWT, which was noted as a minimum depth due to the attenuation of seismic signal with depth, combined with large seismic chimneys immediately below the mud volcanoes. Pockmarks were classified into groups according to their main source in the seismic cross-sections below and these classifications were added to the table of pockmark attributes in ArcGIS.

Due to the quality of the seismic data, particulary around salt, it is not always clear to see where a pipe would extend to, or be sourced from. Equally, it is not always clear what the source of a pockmark is – a pipe is not always imaged, particularly when it is sub-seismic in scale or no longer active. This was particularly true in the studied salt mini-basins where the depth of source is difficult to predict and may be underestimated. Seismic chimneys are only present below the areas identified by the BOEM to be actively leaking gas, as well as below mud

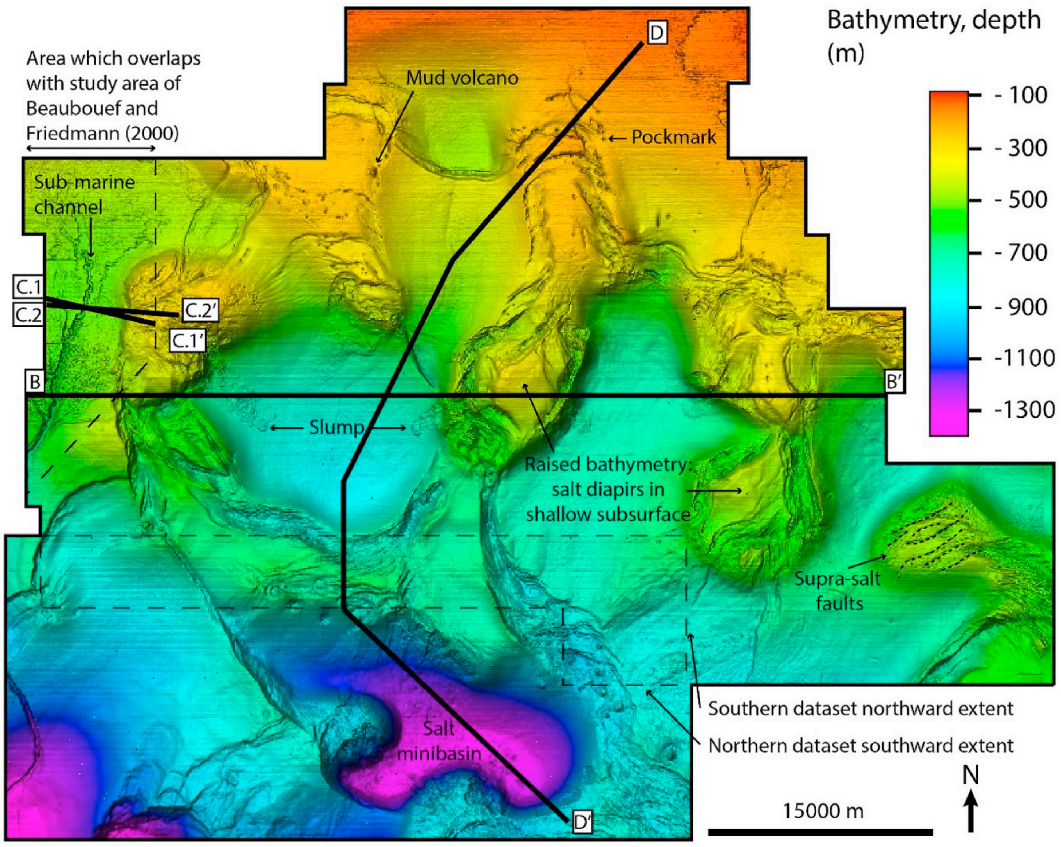

Fig. 5. Bathymetric map highlighting main seafloor features including pockmarks, mud volcanoes, faults, slumps and channels. Seismic line B–B′ is shown in Fig. 6; lines C.1-C.1′ and C.2-C.2′ are shown in Fig. 8; line D-D′ is shown in Fig. 13.

volcanoes. Such processes may be occurring over a greater area, and not only focused in a pipe.

3.5. Spatial analysis and geostatistics

The spatial distribution of pockmarks and mud volcanoes was investigated to better understand the relationship between fluid escape at the sea floor and structures at depth. Spatial analysis was conducted visually by overlaying the delineated pockmarks and mud volcanoes with the seafloor anomalies interpreted by the BOEM. The 'Point Density' Tool in ArcGIS was used to calculate the density of pockmarks per km^2, and results were plotted on a variance map of the sea floor (Fig. 16).

Statistical data was computed based on the morphological results of the BGS Seafloor Mapping Toolbox by plotting box plots, calculating percentages of pockmarks in different settings and cross plotting morphological attributes.

In our analysis, the 'Next Nearest Neighbour Index (Rn)' (Equation (1)) is a first order statistic which determines whether the points (pockmarks) are clustered (Rn < 1), random (Rn = 1) or dispersed

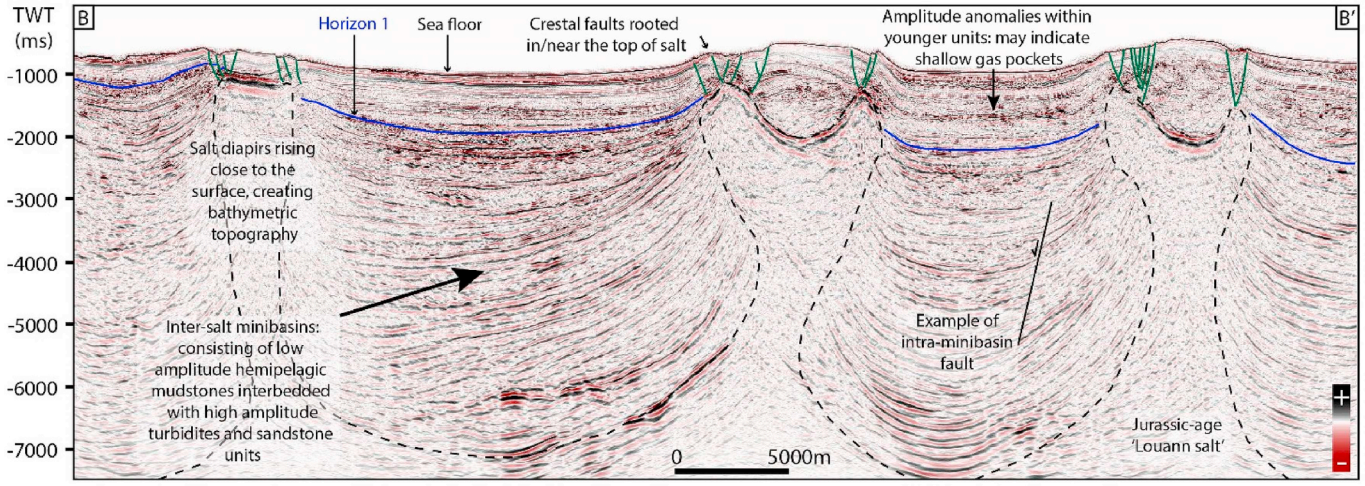

Fig. 6. Representative E-W seismic line through the salt minibasins and salt diapirs, highlighting the main structure of the study area. Location of seismic line is shown in Fig. 5.

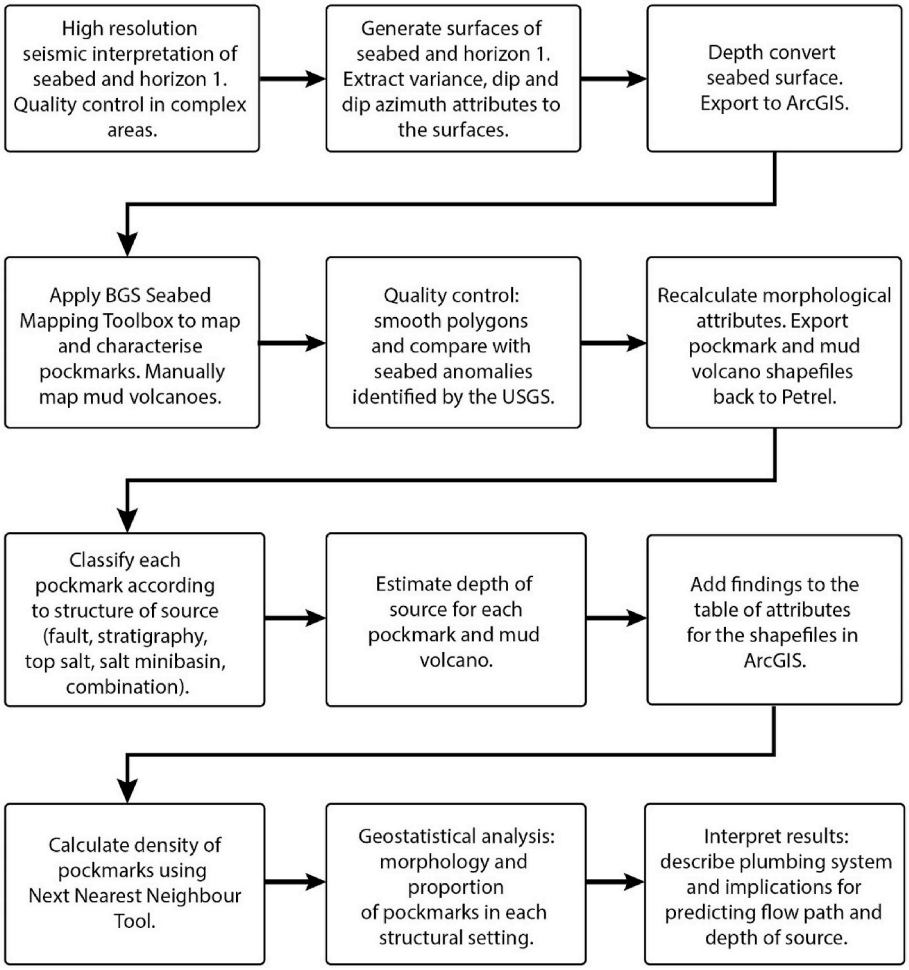

Fig. 7. Methodology workflow. An integration of Petrel (for seismic interpretation) and ArcGIS (for mapping anomalies and spatial analysis) was used.

Table 1
Summary of the input parameters used for the Seafloor Mapping Toolbox in ArcGIS. Parameters were chosen, after trial and error, to be above the vertical resolution limit of detectability so as to keep the number of artefacts mapped and number of missed pockmarks to a minimum. Minimum width equals the minimum horizontal bin spacing, whilst the width:length ratio is adopted from Gafeira et al. (2012). Buffer distance extends the polygon, compensating for the fact that the vertical relief threshold cuts the uppermost part of each pockmark. Buffer distance was chosen to be half of the minimum width (Geldof et al., 2014).

Input Parameters	Values
Cutoff vertical relief	2 m
Minimum vertical relief	5 m
Minimum width	20 m
Minimum width:length ratio	0.2
Buffer distance	10 m

(Rn > 1) (Clarke and Evans, 1954).

$$Rn = \frac{\bar{D}\ (Obs)}{0.5\sqrt{\frac{a}{n}}} \quad (1)$$

Where $\bar{D}$ (Obs) is the mean observed nearest neighbour distance, n is the number of pockmarks and a is the aerial extent of pockmark coverage in the study area. This latter parameter was determined by subtracting the area obtained from the density calculation with 0 pockmarks per km^2 from the total study area. This statistical parameter was calculated using the 'Average Nearest Neighbour' Tool in ArcGIS.

4. Seismic stratigraphy

The seismic stratigraphy of the study area is summarised in Fig. 8. The Jurassic Louann salt forms irregular-shaped, diapiric structures with chaotic internal seismic character that extend vertically from the bottom of the survey towards the sea floor between discrete minibasins. The strata in the deepest parts of the minibasins are generally characterised by low amplitude, continuous seismic reflections that are upturned towards the edges of the minibasins by the salt. These units represent Mio-Pliocene deep-marine siliciclastic, most likely hemipelagic mudstones (Galloway, 2008). Wedge geometries with onlap and infill are apparent down to 6 s TWT, a consequence of the different growth rates across distinct salt diapirs, indicating that salt has been mobile since at least the Miocene. However, the seismic quality decreases considerably with depth due to the high absorption of acoustic energy by the Louann salt (Fig. 6; 8).

Seismic facies interpretations were correlated with those of Prather et al. (1998) and Beaubouef and Friedmann (2000). The study area of Beaubouef and Friedmann (2000) overlaps the study area by ~8 km on its western edge and was, therefore, deemed a reliable reference given the absence of well data. The authors describe these minibasins as being filled rapidly with pronounced stratigraphic cyclicity, especially during the late Pleistocene.

Three key seismic facies filling salt minibasins were identified by Beaubouef and Friedmann (2000) within the initial 1s TWT below the

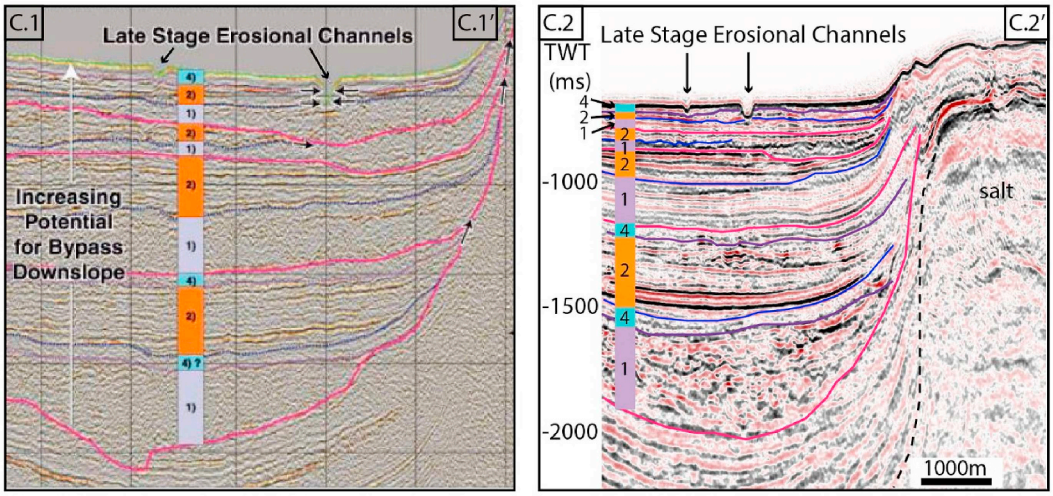

Fig. 8. Comparison between the 2D seismic line given by Beaubouef and Friedmann (2000) (C.1-C.1′) and the approximate equivalent line in the seismic survey available for this study with the best match (C.2-C.2′). Location is shown in Fig. 5. Although some differences may be present, overall features are clear: generally chaotic facies (seismic facies type one) correspond to mass-transport complexes (MTCs); higher amplitude regular facies (seismic facies type two) are 'DLCs' - distributary channel-lobe complexes; whilst lower amplitude continuous facies (seismic facies type four) are 'DCs' – hemipelagic drape complexes. Seismic facies type three is omitted here for consistency, because in the study by Beaubouef and Friedmann (2000), it represents a different facies that is not apparent in this part of the basin.

sea floor, corresponding to the late Pleistocene (Fig. 8). Facies one (1) consist of low amplitude, chaotic seismic reflections, which are interpreted as mud-rich slumps, slides and debris flows of mass-transport complexes (MTCs). Facies two (2) exhibits high amplitude and continuous seismic reflections, with onlapping, locally erosional geometries, and fan-shaped or distributary map patterns. These are interpreted to be sediment gravity flows, which are collectively called 'distributary channel-lobe complexes' (DLCs) and are considered to be the richest in sand with the greatest reservoir potential (Beaubouef and Friedmann, 2000). Facies three (3) consist of thin, highly continuous seismic units interpreted to represent hemipelagic mudstones deposited during periods of abandonment and sediment starvation – also called hemipelagic drape complexes (DCs) (Beaubouef and Friedmann, 2000). In Fig. 8, this is labelled facies four (4), to be consistent with Beaubouef and Friedmann (2000). All these slope depositional systems were abandoned and draped by a condensed interval of hemipelagic mud during the Holocene transgression and the present-day sea-level highstand.

5. Seismic interpretation of fluid flow features

5.1. Seismic interpretation of amplitude anomalies

Seismic interpretation of the sea floor revealed a deformed bathymetry containing depressions (pockmarks), fault scarps, mud volcanoes and sediment slumps (Fig. 5; Fig. 9). These features are confirmed by previous work done by the BOEM and their classification of seafloor anomalies.

Fig. 10 shows seismic-based evidence of high-amplitude anomalies within the salt minibasins – often high-amplitude reflections within normal reflections. These are typically associated with higher reflectivity and chaotic seismic units (e.g. MTCs) as well as some examples of channel-shaped bright spots in seismic section. Pockmarks are not associated with most of these anomalies. Rare cases of polarity reversal and flat spots have also been found within the sediments in the minibasins, which are interpreted to indicate fluid contacts – likely gas-on-water (Fig. 10a and c).

5.2. Interpretation of mud volcanoes

A total of 62 circular-shaped seafloor mounds were manually mapped. At least 12 mounds are interpreted to be mud volcanoes according to the BOEM data, whilst other mounds have distinct seismic characteristics - including a vertical seismic chimney below the anomalously high-amplitude sea floor and cone-like seafloor structure (Fig. 11). Matching the descriptions of other authors (e.g. Brown, 1990; Chen et al., 2015), these mounds are therefore interpreted as mud volcanoes. The mud volcanoes are larger than the pockmarks, with widths ranging from 135 to 725 m (Fig. 12). The BOEM identified at least 12 mounds to be actively leaking hydrocarbons and brine.

The mud volcanoes are found along the edges of salt diapirs across the study area, whilst 19 cluster in the southern part of the study area where very few pockmarks have been identified. In some cases, mud volcanoes appear to be sourced from the top of salt (source depth from 400 to 1000 ms TWT). In general, seismic chimneys appear to extend from at least 600–2000 ms TWT below mean sea level, into the bottom of the minibasins.

5.3. Dip and dip azimuth of salt minibasins

Dip and dip azimuth maps show the degree and direction of dip (respectively) of the sea floor and Horizon 1 at depth (Figs. 13 and 14). The dips of the minibasin stratigraphy adjacent to the salt structures increase considerably with depth due to the diapiric nature of the salt, causing the bedding to be upturned at the edges of salt to 10°–30° (Figs. 13a and 14a). Azimuths of the sea floor and Horizon 1 are predominantly to the south, between 150° and 225°. The direction of along-horizon migration is opposite to azimuth, therefore the regional migration is predominantly to the north, with locally south-migrating pathways. The presence of pockmarks decreases towards the south, perhaps reflecting the regional migration to the north invoked here, whilst mud volcanoes are present across the study area but concentrated in the south. The minibasins become deeper and edges are steeper in the south of the study area (Fig. 15), which coincides with the cluster of 19 mud volcanoes shown in Fig. 9.

6. Spatial distribution of pockmarks and BOEM anomalies: relationship with subsurface structure

Pockmarks are abundant in areas of relative raised bathymetry – a result of the growth of underlying salt diapirs – and occur particularly close to linear features corresponding to faults. Fig. 16 shows a 'heat

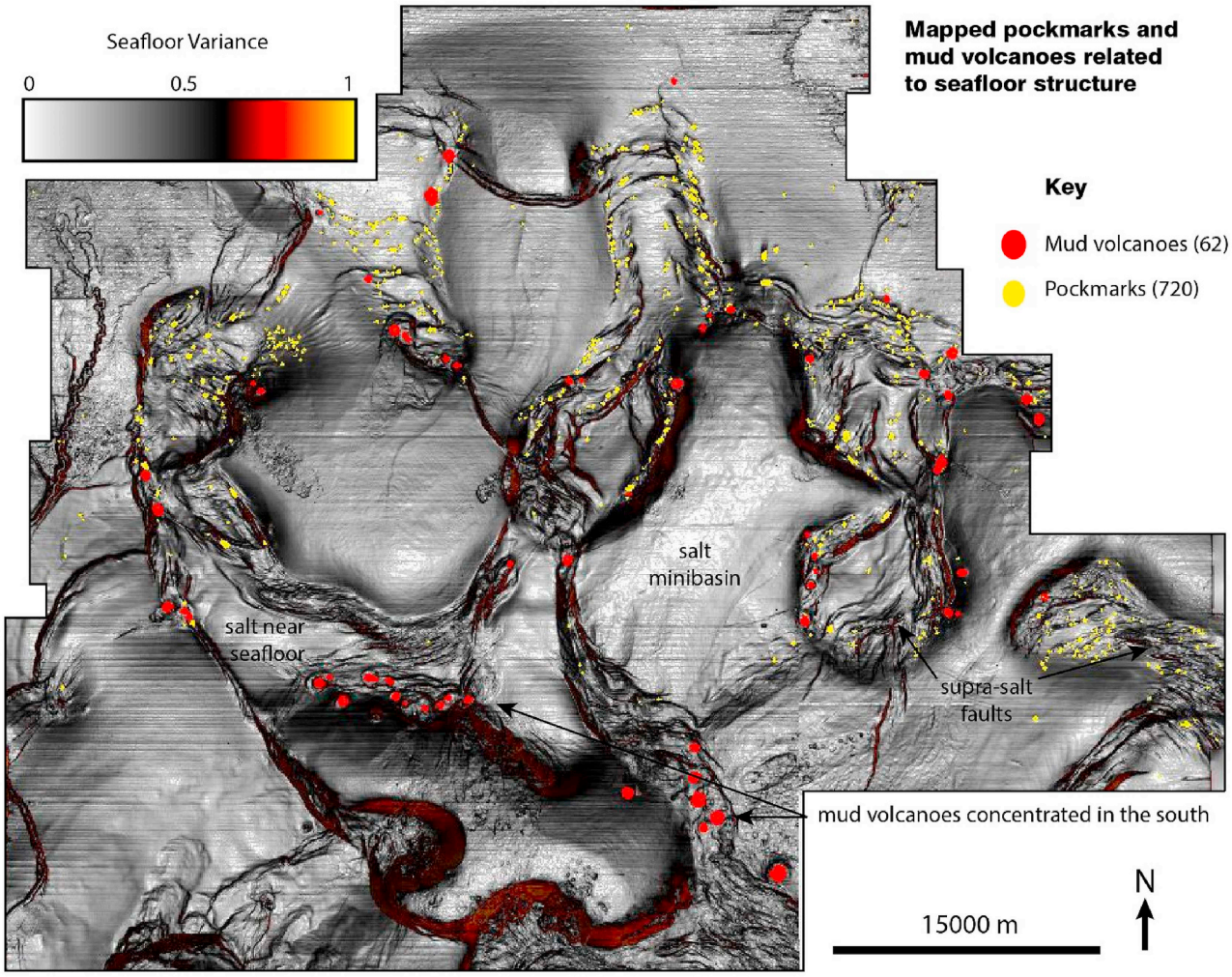

Fig. 9. Seafloor variance map which emphasizes seafloor structure, in particular faults; salt minibasins; salt diapirs close to the sea floor; 720 pockmarks (yellow) and 62 mud volcanoes (red) mapped using ArcGIS in this study. Pockmarks and mud volcanoes are focused above and along the edge of salt structures and where faults meet the sea floor. (For interpretation of the references to colour in this figure legend, the reader is referred to the Web version of this article.)

map' of the interpreted pockmarks, quantifying the density of pockmarks between 0 and 15 pockmarks per km^2. In the total area surveyed (2031 km^2), 82.5% contains 0 pockmarks per km^2, whilst 8.9% contains only 1 pockmark per km^2. As little as 0.02% of the study area contains a density of 11–15 pockmarks per km^2. Visually, the pockmarks appear clustered. This is validated statistically by the Next Nearest Neighbour ratio (Rn). The observed mean distance between any two pockmarks is 470 m and Rn = 0.56 with a Z-score of −22.6, meaning there is less than 1% likelihood that this clustered pattern is the result of a random process. These values illustrate two key points: a) that the pockmarks are clustered in small focal areas relative to the size of the study area, and b) these densities are low compared with data from other sedimentary basins (Table 2).

Several near-seafloor anomalies are depicted in the BOEM data (Table 3; Fig. 17). As with the mapped pockmarks, these anomalies occur near faults and above the salt structures, indicating focused fluid pathways in these areas. The presence of natural gas plumes and oil slicks confirms that hydrocarbons are leaking to the sea floor, as opposed to being overpressured brines or biogenic gas. Gas plumes are associated with pockmarks, indicating that these are active, established pathways of hydrocarbons to the sea floor (Fig. 17). The high- and low-amplitude anomalies representing possible oil leakage points are located where faults meet the sea floor, suggesting that these are the main leakage pathways for oil.

Pockmarks were classified into five (5) different settings that correlate with the type of source at depth: a) stratigraphic carrier beds located above the salt diapirs, indicated by an amplitude anomaly or pinch-out of beds along a structure such as an anticline; b) pockmarks sourced directly from the top of salt; c) pockmarks located within a fault scarp at the surface, whereby the fault is rooted in a carrier bed above salt, or on the top of a salt diapir; and d) pockmarks sourced from carrier beds in adjacent salt minibasins (Table 4). The fifth group of pockmarks accounts for those generated by a combination of sources; in some areas of the dataset it is difficult to interpret the underlying structure. For instance, inlines may show no shallow salt and the pockmarks appear to occur in salt minibasins, whilst salt is well imaged in adjacent crosslines. Fig. 18 shows examples on seismic of pockmarks from each of these settings. Approximately 96% of pockmarks are associated with salt diapirs at depth, with sources predicting to be top salt (17%), stratigraphic units above the salt (21%), or supra-salt faults (49%). The pockmarks located within fault scarps at the sea floor are not associated with vertical pipes, indicating that fluid flow occurred along the fault plane. This flow was still focused and with a degree of explosiveness as surface material within the fault scarp was excavated to form distinct pockmarks on the sea floor.

The pockmarks located within the minibasins (4%) are interpreted to have been sourced from high-amplitude anomalies in the shallow stratigraphy (Fig. 18d).

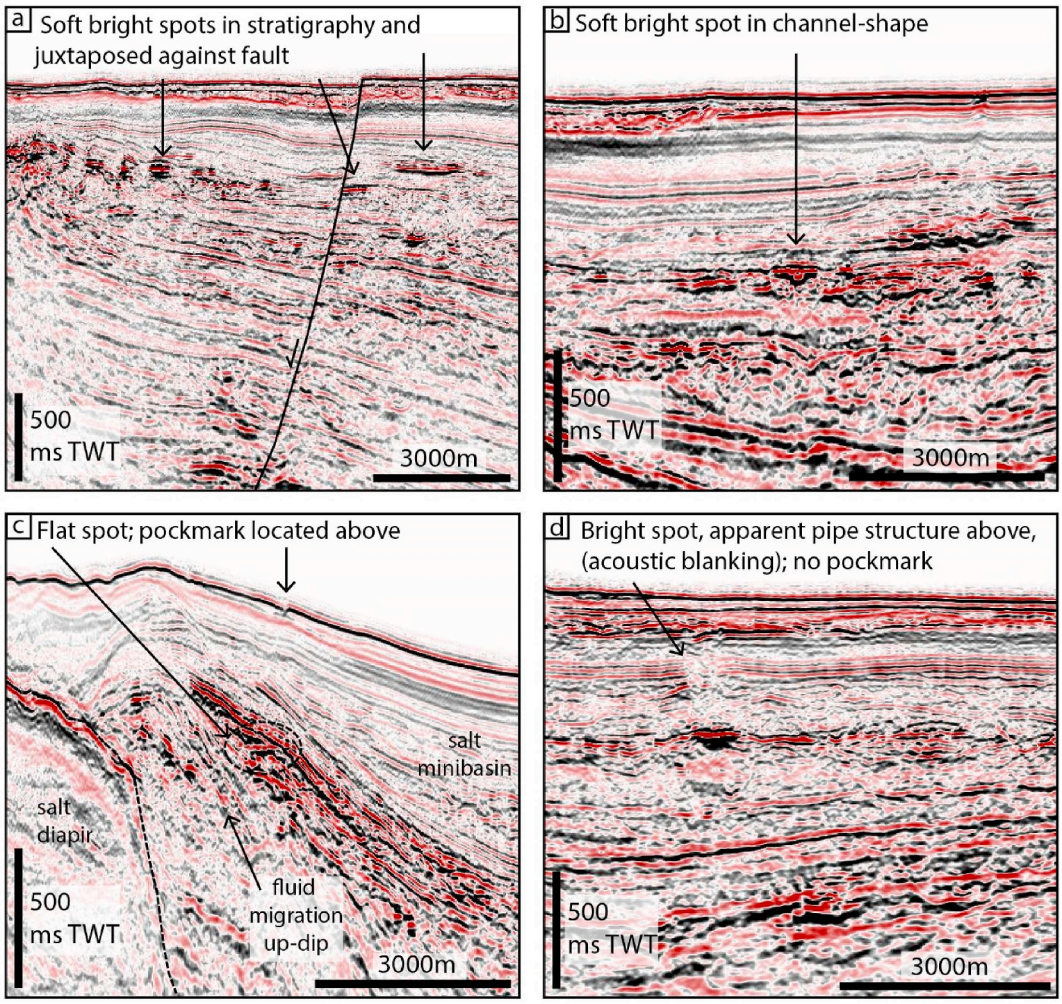

Fig. 10. Examples of different amplitude anomalies in the salt minibasins: a) soft bright spots in stratigraphy and bright spot juxtaposed against fault; b) soft bright spot with a channel-like shape; c) flat spot, with pockmark located above, revealing a possible association; d) bright spot with acoustic blanking above, but no visible pockmark.

7. Source depth and morphological analysis of pockmarks

Box plots were generated for the estimated depth of source for the pockmarks in each pockmark source category (Fig. 19). The plot shows a range of depths from 100 to 1750 ms TWT, with the data clustered between 400 and 800 ms TWT. The depths of source are not clearly distinct across different structures, and given that most of the pockmarks are associated with the top salt horizon, the depth is a function of the growth of the salt diapir to the sea floor.

Vertical relief ranges from 1 m to 41 m whilst width ranges from 20 m to 400 m, similarly to normal pockmarks measured in other parts of the world (Table 2). Fig. 19 also illustrates the distribution of vertical relief across the structures, which all seem to cluster between 3 m and 15 m. The median value for fault-sourced pockmarks is slightly greater (9.5 m) than for the other categories (5–7.5 m), and the range of data and maximum values for salt-related pockmarks are greater than for those in the minibasins. However, the morphology of pockmarks does not clearly correlate to the fluids structural sources.

Pockmark and mud volcano width was plotted against depth of source (Fig. 20). Pockmark widths are clustered below 200 m across the range of depths, from 50 to 1200 ms TWT. In this study, depth of source does not directly control the size of the pockmark, as shown by the horizontal trendline. In contrast, there is a trend of increasing width of mud volcanoes with increasing depth.

Pockmark eccentricity is represented by the width:length ratio: the greater the ratio, the more spherical the pockmark (Fig. 21). The mean width:length ratio is 0.79, however the majority of the data lies above this value, indicating high sphericity across the structures which suggests that pockmarks have not been deformed by bottom currents or side collapse (Judd and Hovland, 2007), and are assumed to be very recent features. There is a greater range of width:length ratio for the pockmarks found in fault scarps. Highly eccentric pockmarks (width:length ratios down to 0.25) elongated parallel to the strike of faults further supports the interpretation that fluids are utilising the faults as flow pathways to the surface.

8. Discussion

8.1. Hydrocarbon plumbing systems at East Breaks

The results of the seismic and GIS mapping show that the pockmarks are concentrated above salt diapirs, whilst mud volcanoes are located at edges of salt or at fault intersections. Statistical and spatial analysis confirmed that the salt diapirs are the dominant structures for focusing fluids from depth, with supra-salt faults including crestal, roller and ramp faults (Rowan et al., 1999) as pathways for fluids to the surface.

Due to the deep burial of source rocks in the Gulf of Mexico, few source rocks have been penetrated during drilling on the continental slope. The petroleum systems of the field 'East Breaks 160–161' have been previously described (Armentrout, 1999); here, the critical

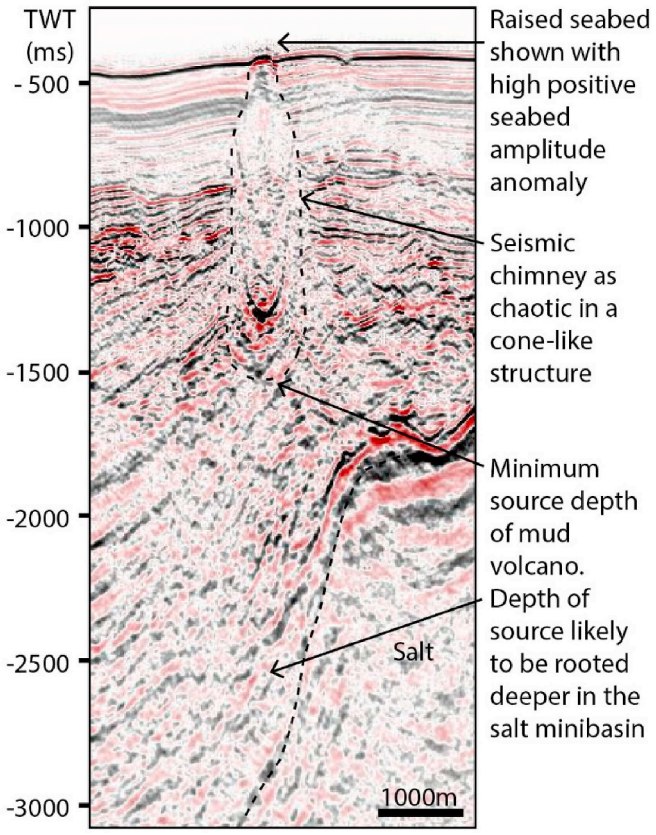

Fig. 11. Example of a near-seafloor structure interpreted to be a mud volcano: large seismic chimney, high positive amplitude at the sea floor, raised seafloor bathymetry. Depth of source interpreted is a minimum, as the chaotic and poorly resolved seismic signal at depth makes it difficult to interpret the true depth of source.

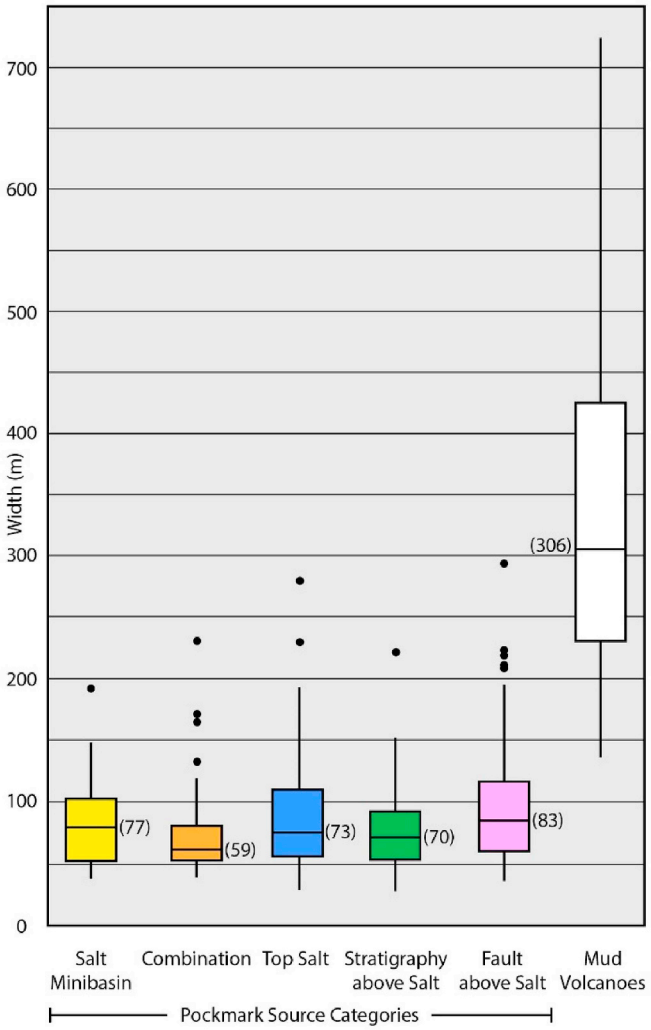

Fig. 12. Box plot showing the widths of the pockmarks across the different source categories and mud-volcano widths. The mud volcanoes are on average 3–4 times larger than pockmarks in the study area. Black dots are outliers, and median values are labelled.

moment is related to a source rock predicted to be within the Miocene strata (Dow et al., 1990). The Miocene source rocks would not yet have produced large volumes of gas or gas condensate, which may explain the lack of volatile hydrocarbons in the produced crudes at the field 'East Breaks 160–161', compared to the majority of fields in the northern Gulf of Mexico (Thompson, Kennicutt and Brooks II, 1990). Gross et al. (1995) noted that the potential source rock occurs within the Upper Jurassic (Tithonian) and, for this to be plausible, generation must have been delayed until very recently. Alternatively, hydrocarbons from the Tithonian source migrated to primary reservoirs during the early Cenozoic and to secondary reservoirs and the sea floor over the course of the last 1 Ma after salt welds formed, which provided the fluid bypass pathway (McBride et al., 1998).

The uppermost 1.0 s TWT of sediment are considered to be Pleistocene to Recent in age – Beaubouef and Friedmann (2000) proposed that the deposition of these units occurred within the latest Pleistocene, over approximately 100 kyr, highlighting the rapid deposition and fill of the minibasins. This also implies that fluid flow features are modern, less than 100 kyr and fluid migration occurred rapidly. Many are active at present, as the BOEM data notes the presence of ascending gas within the water column, clustered around pockmarks (Fig. 17). Oil slicks and gas plumes confirm that the pockmarks are not simply a result of rapid compaction and dewatering of sediments.

Two main fluid flow mechanisms are invoked in this work (Fig. 22). Primarily, sub-salt hydrocarbons migrated across salt welds and into minibasin stratigraphy. Migration occurred along salt, or along carrier beds which are tilted up towards the salt diapir walls. The fluids meet the sediment-salt interface and are diverted up the flow path of least resistance, along the salt surface by boundary flow (Jackson and Hudec, 2017). Fluids flow vertically and horizontally across the top of diapirs. Here, they continue to flow vertically to the surface along faults – in which case, we do not see the pipes. Alternatively, fluids concentrate in shallow reservoirs, accumulating in volume until the pore volume pressure exceeds overburden pressure and a fracture network forms to the surface, forming a pipe which terminates in a pockmark at the sea floor. Sediments under tension such as those above salt diapirs provide migration pathways for pipes to form (Judd and Hovland, 2007). We interpret that pipes formed from the salt diapir flanks, the tops of salt diapirs, and from carrier beds above the salt. It is also possible that hydrocarbons were escaping to the sea floor much earlier than the last few thousand years, but without the formation of pockmarks. Judd and Hovland (2007) noted that a stable sea floor with no large-scale active erosion or deposition is required for pockmarks to form, and up until the Holocene transgression, this study area was experiencing very high rates of deposition, evidenced by the thick Pleistocene sediments.

Secondly, diffusive fluid flow may also have occurred vertically across the strata within the minibasins – or along deep-seated faults within minibasins (Fig. 6). Hydrocarbons could accumulate in sand-rich zones within mass-transport complexes. Bright spots throughout the minibasins indicate the abundance of shallow gas pockets. These may be hydrocarbons found in stratigraphic traps, particularly buried

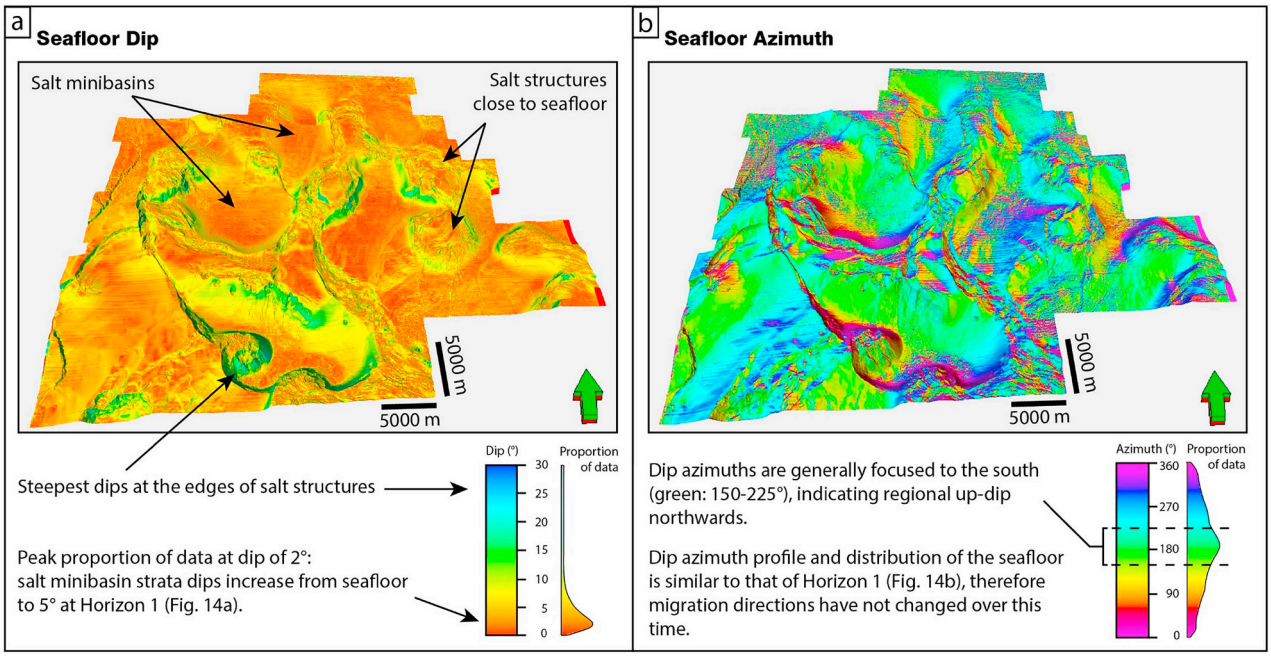

Fig. 13. a) Sea floor dip map showing small dips in the minibasins, increasing in steepness towards the edges of salt structures; b) Sea floor dip azimuth map showing predominantly southwards-dipping sea floor. Fig. 13 is represented in 3D. See Fig. 9 for locations of mud volcanoes and pockmarks relative to the sea floor in 2D. See Fig. 14 for comparison with Horizon 1.

channels (Fig. 10b). Fig. 10c shows one of a few examples of interpreted flat spots – a fluid contact, which suggests the presence of hydrocarbons as shallow as 1 s TWT below the sea floor within the minibasins. The shallow strata are also tilted due to the ongoing salt movement, so hydrocarbons could be migrating laterally up-dip towards the salt flanks near the surface. Alternatively, the bright spots may be a result of biogenic gas, which is also prolific in the Gulf of Mexico due to high total organic carbon input and high sedimentation rates, particularly in the salt minibasins (Boswell et al., 2012; Hutchinson et al., 2011). In the Gulf of Mexico, gas hydrates can form from biogenic or thermogenic gas under high pressure and low temperature conditions, therefore typically close to the sea floor and at water depths of at least 300–600 m (Hutchinson et al., 2011). If gas hydrates are present in the study area, they could be acting as seals in the salt minibasins (Speight, 2011) as

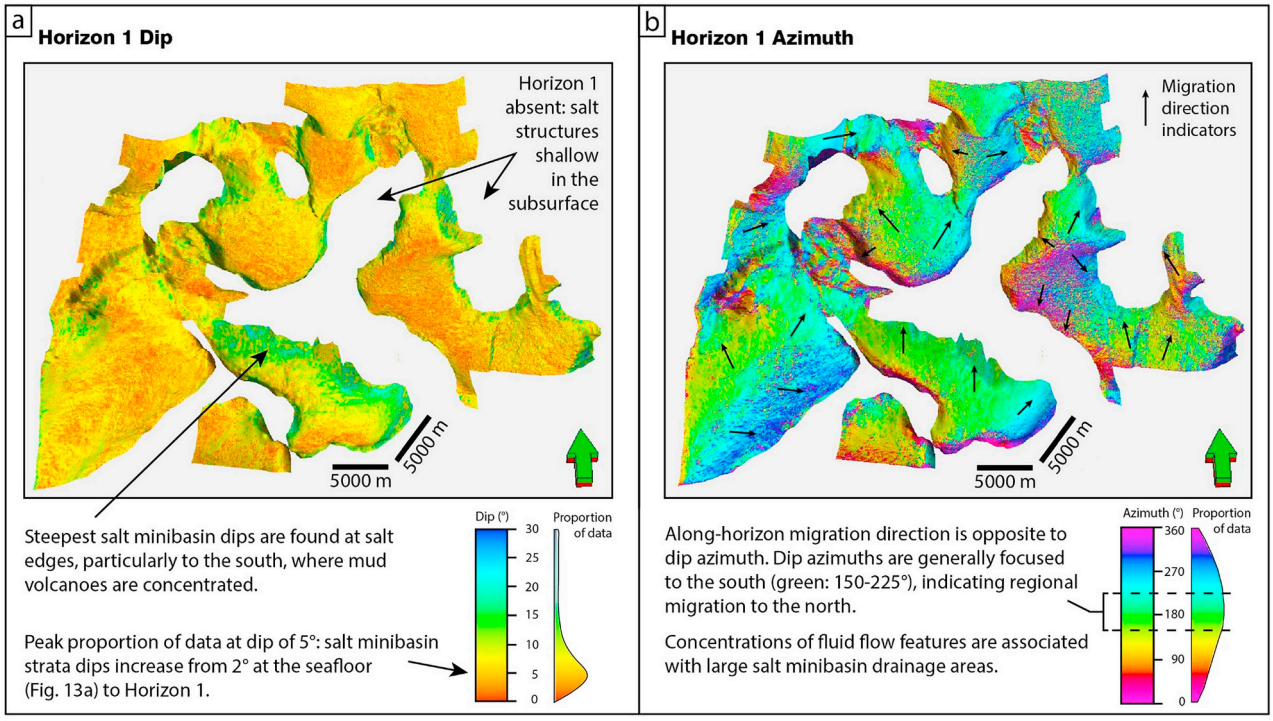

Fig. 14. a) Horizon 1 dip map with dips steeper than those at the sea floor; b) Horizon 1 dip azimuth map. Direction of fluid migration along carrier beds is opposite to azimuth, therefore regional northern migration is evident, indicated by arrows. Fig. 14 is represented in 3D. See Fig. 9 for locations of mud volcanoes and pockmarks relative to sea floor in 2D. See Fig. 13 for comparison with sea floor.

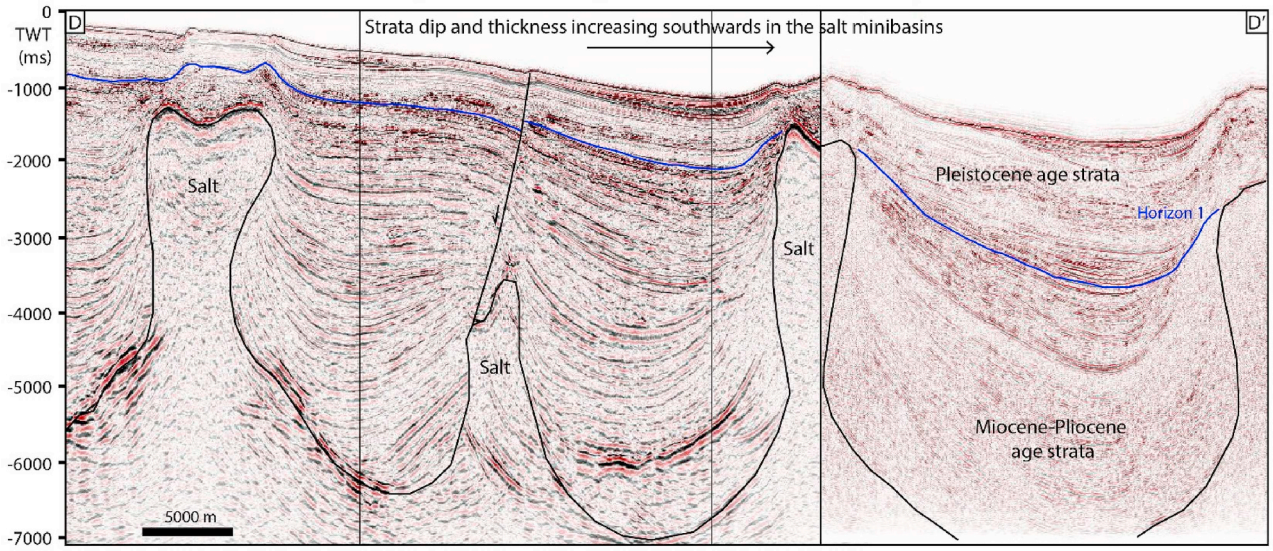

Fig. 15. Composite seismic line through the salt minibasins in the study area, from north to south, showing increasing thickness and dip of salt minibasin stratigraphy to the south. Location of line is shown in Fig. 5.

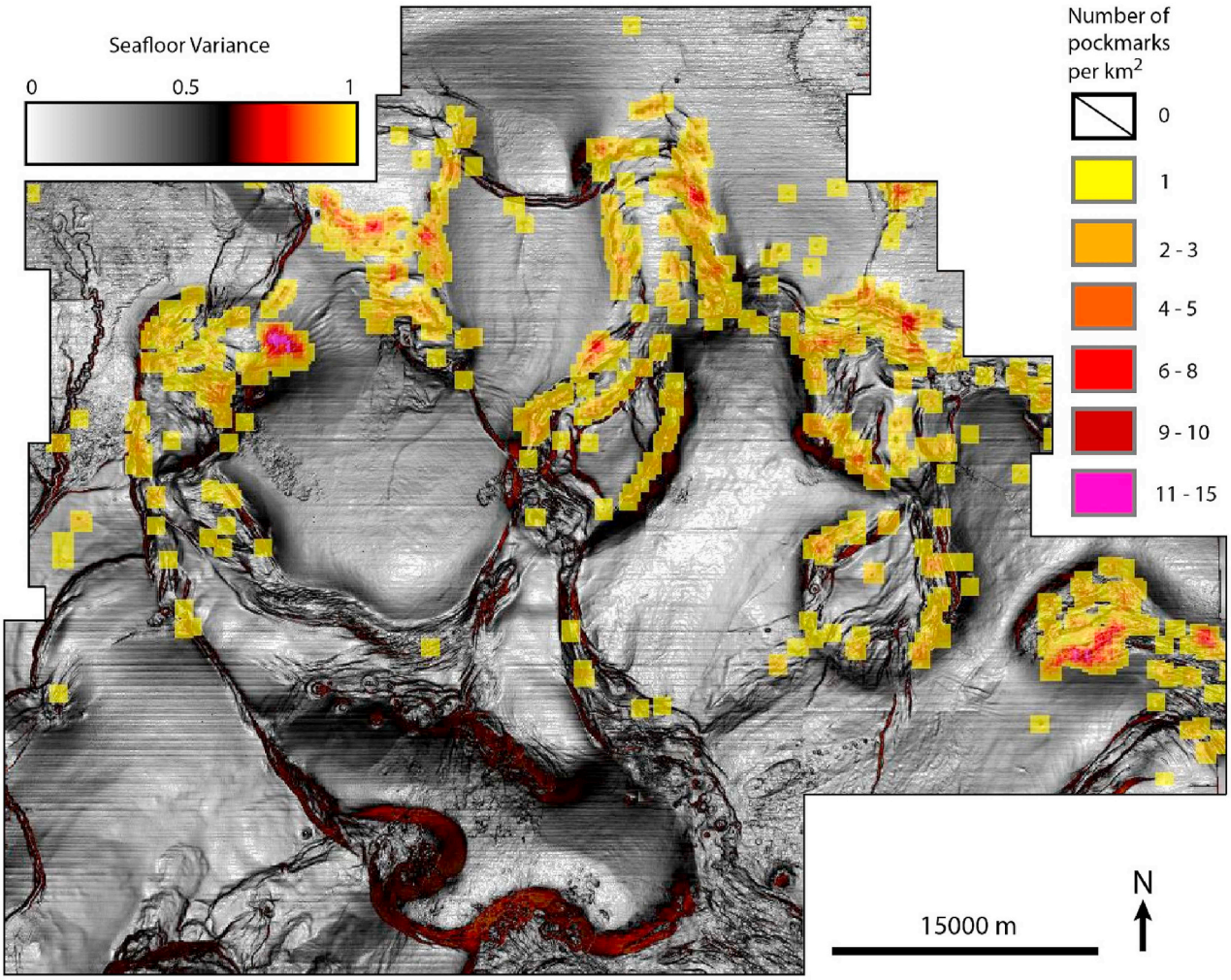

Fig. 16. Seafloor variance map, overlain with the density of pockmarks, ranging from 0 to 15 per km^2. Pockmarks are concentrated along faults above areas of raised bathymetry, coinciding with shallow salt structures below. Pockmarks are mostly absent in the southern part of the study area, where mud volcanoes predominate.

Table 2
Examples of the density of pockmarks per km^2, average width and vertical relief of pockmarks from other papers and this dataset.

Paper	Density /km^2	Width (m)	Vertical Relief (m)	Location
Moss et al. (2012)	100–600	16	0.5	Rosetta Region, Eastern Slope, Western Nile Deep Sea Fan
Tasianas et al. (2018)	n/a (elliptical pockmarks) 600–700 (unit pockmarks)	Up to 300 Up to 20	Up to 12 Up to 1	Snøvit Area, Hammerfest Basin, SW Barents Sea
Hasiotis et al. (1996)	80–150	25–250	0.5–15	Gulf of Patras, northern Peleponnese, Greece
Judd and Hovland (2007)	10–40	50–150	1–3	Witch Ground Basin, North Sea
Judd and Hovland (2007)	Up to 160	20–200	1–35	Gulf of Maine, USA
This paper: pockmarks	*0–15*	*20–400*	*1–41*	*East Breaks, northern Gulf of Mexico, USA*
This paper: mud volcanoes	*0–2*	*135–725*	*2–55*	*East Breaks, northern Gulf of Mexico, USA*

few pockmarks (4% of total mapped) are evident here. In such a case, biogenic or thermogenic gas could accumulate below gas hydrates and migrate up-dip towards the salt diapirs and source the pockmarks.

8.2. Relationship amongst pockmarks, mud volcanoes, underlying structures and depth of source

No clear correlation is seen between the size or morphology of pockmarks and structures or depth of source. It was hypothesized that larger pockmarks would have deeper sources, as greater overpressure is required to produce a larger explosive force that excavates more material at the sea floor. However, there are several factors that can influence the size of the pockmarks in the study area, the combination of which may have resulted in a non-descript relationship between pockmark size and depth of source or structural source type.

The size of pockmarks depends partly on the volume of gas that has accumulated – the larger the volume, the greater the overpressure and explosive force to form the pockmark. A shallower source can still produce a large pockmark if sufficient volume of gas is expelled. For a pockmark to have formed from a deeper source, a higher gas pressure (volume) is required to overcome the higher overburden pressure. Energy dissipates as fluids migrate vertically (particularly if more porous media are encountered and gas migrates laterally), and in such a case, gas may not reach the surface (Fig. 10d). However, fluid volume increases due to gas expansion and exsolution as it rises, causing the upward buoyancy force to also increase and form a pockmark (Judd and Hovland, 2007).

This particular study does not establish a clear correlation between the depth of the reservoir hosting fluids which formed the pockmarks, and pockmark morphology. In most cases, the source of the pockmarks was considered to be an amplitude anomaly in sub-surface strata, the crest of an anticline, or the top of salt. However, as the seismic profiles beneath the mud volcanoes appear to show seismic chimneys extending well below the top of the salt diapirs (on the flanks), we expect mud volcanoes to reflect relatively deeper fluid flow, potentially sourced at several kilometres depth. The mud volcanoes are substantially larger seafloor features compared to the pockmarks, where each one formed from a larger catchment area at depth compared to the pockmarks in

Table 3
Summary of the main seep anomalies detected and mapped by the BOEM, and their corresponding descriptions.

Anomaly Type	Description	Observations
Plumes	Natural gas plumes in the water column as detected by the RV Okeanos Explorer's EM302 multibeam sonar in 2011, 2012, and 2014. 400 foot diameter circles to indicate the uncertainty of the exact seep location on the sea floor, which varies with water depth.	Six main clusters, all above salt and near faults. Three clusters are associated with mapped pockmarks. One is within a fault. One is by a positive seep anomaly. One is by a negative seep anomaly.
Pockmarks	Circular-oval depressions interpreted to be created by the removal of sediment through rapid, and possibly, explosive gas expulsion. Few pockmarks have visible active migration pathways on vertical seismic profiles, but most appear to be dormant and without discernible active migration. Rapid expulsion is interpreted to be exclusively gas and appear to be purely destructive due to the removal of sediment. No sediment, brine, or oil expulsion has been observed during direct observations.	447 mapped by the BOEM.
Mud Volcanoes	Cones of sediment typically on low slopes that are built at high flux sites that do not exhibit high positive amplitude response. The rate of flux at the expulsion sites is too rapid for bacterial consumption of the hydrocarbons to convert them to authigenic carbonate hardgrounds, thus sessile chemosynthetic organisms and corals are usually not found on these features. These are unconfirmed by direct observation.	Twelve mapped by the BOEM.
Positive seep anomalies	High, positive seafloor amplitude anomalies interpreted in seismic, which have not yet been confirmed as seep-site hardgrounds.	309, irregularly shaped polygons mapped by the BOEM, typically along faults or near pockmark locations.
Positive seep anomalies – possible oil	High, positive seafloor amplitude anomalies interpreted in seismic, located directly below sea surface oil slicks, or within one water depth's distance. Not directly observed to be seeping oil, but possible oil seeps due to proximity to oil slicks.	16 were mapped by the BOEM, located along faults above salt.
Negative seep anomalies	Anomalously low, positive seafloor amplitude anomalies interpreted in seismic. The most active of this type show a phase reversal – a negative amplitude response of the sea floor – these areas have been observed to have rapid hydrocarbon flux, often with sediment and brine being expulsed in conjunction with the hydrocarbons.	56 were mapped by the BOEM and are all located above salt structures.
Negative seep anomalies – possible oil	Low positive/negative seafloor amplitude anomalies interpreted in seismic, located either directly below sea-surface oil slicks or within one water depth's distance. Not directly observed to be seeping oil, but possible oil seeps due to proximity to oil slicks.	Ten polygons were mapped by the BOEM, in four clusters. Two clusters are in the same area as a gas plume and 'seep anomaly positives – possible oil'.

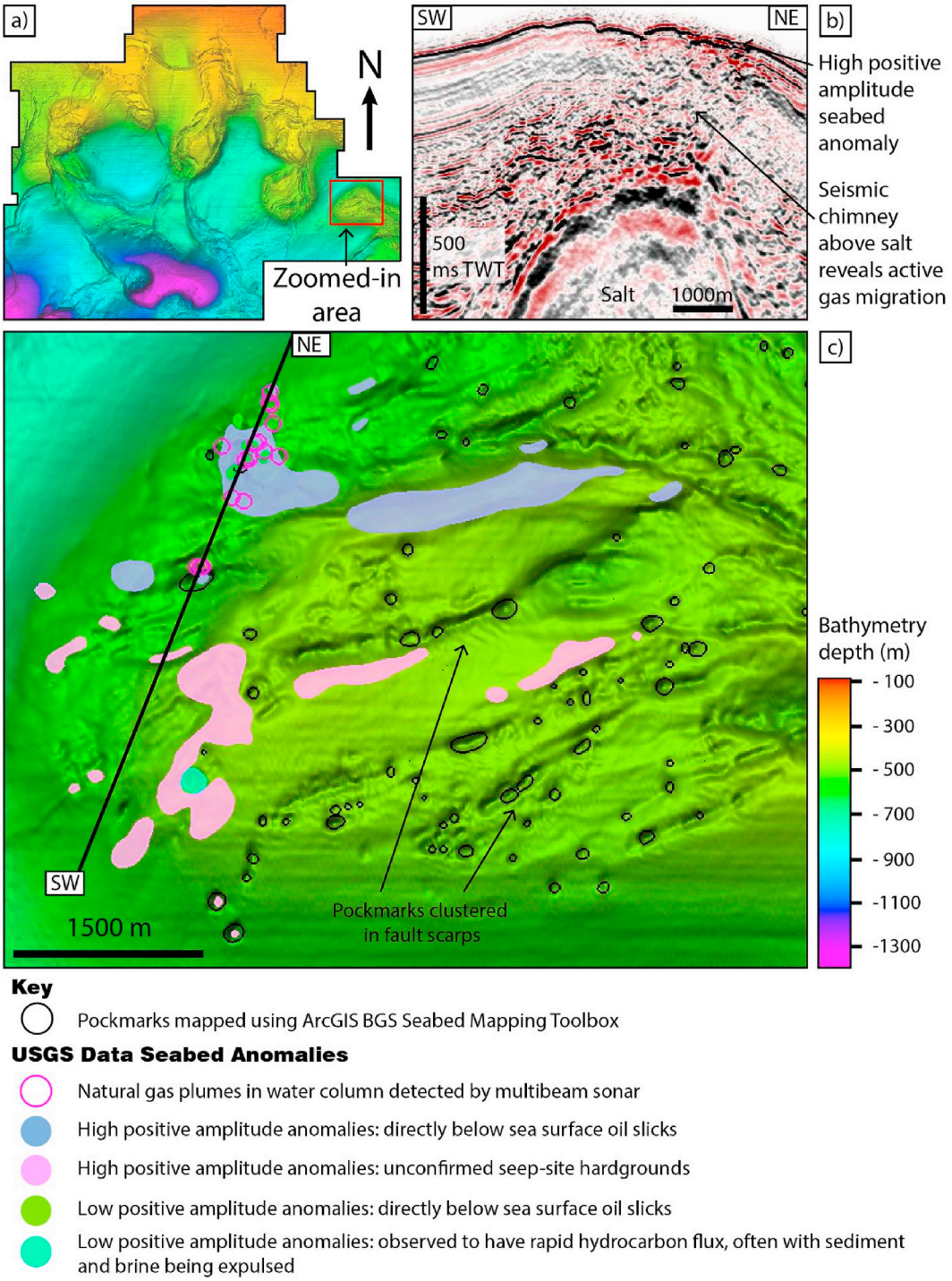

Fig. 17. a) Map of study area showing a zoomed-in region in c). b) NE-SW seismic section showing a gas chimney above a salt diapir, location indicated in c). c) Zoomed-in example of the concentration of seafloor amplitude anomalies (identified by the BOEM) near faults and pockmarks. Natural gas plumes are also shown to be concentrated in these areas, which correspond to chaotic seismic chimneys immediately below. The seismic chimneys may represent active gas migration, or scattering of energy if hardgrounds had formed at the sea floor.

Table 4
Summary of the pockmark source categories, the number of pockmarks found in each category and the number of mud volcanoes in the study area.

	Pockmark source categories					Mud volcanoes
	Minibasin	Combination	Top Salt	Stratigraphy above salt	Faults above salt	
Number of pockmarks or mud volcanoes	31	61	124	154	350	62
% of total pockmarks	4	9	17	21	49	n/a

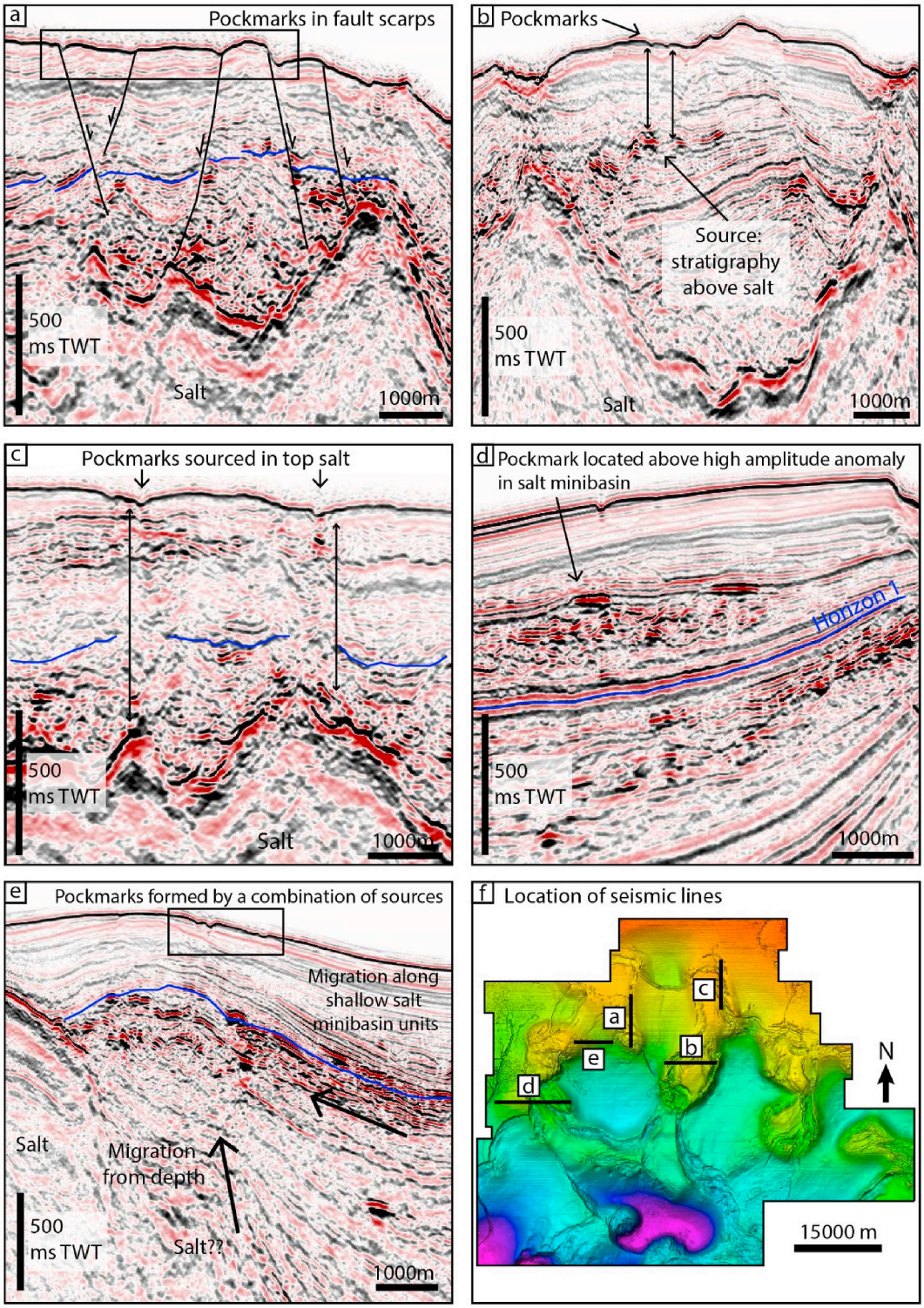

Fig. 18. Seismic examples of the five (5) different source categories: a) pockmarks located in fault scarps; b) pockmarks that appear to be sourced in stratigraphy above salt; c) pockmarks sourced from top salt; d) pockmarks located in salt minibasins sourced from amplitude anomalies; e) pockmarks whose source is difficult to interpret, or may be sourced from a combination of fluids from depth and from shallower salt minibasin units. Fig. 18f) shows the locations of the seismic sections. Horizon 1 is labelled in blue and is absent in Fig. 18b). (For interpretation of the references to colour in this figure legend, the reader is referred to the Web version of this article.)

the shallow subsurface. Huge overpressures are required to form the mud volcanoes, and to mobilize mud from a few kilometres depth to the sea floor. These overpressures were likely supported by a combination of rapid loading of the minibasins and hydrocarbon (particularly gas) migration within overpressured and, therefore, lower density mud units (Judd and Hovland, 2007).

It is apparent that the mud volcanoes are sourced from much deeper strata in the minibasins, particularly in areas where the minibasins are thicker – towards the south of the study area – and coincide with steeply dipping strata that hydraulically feed these seafloor features. In

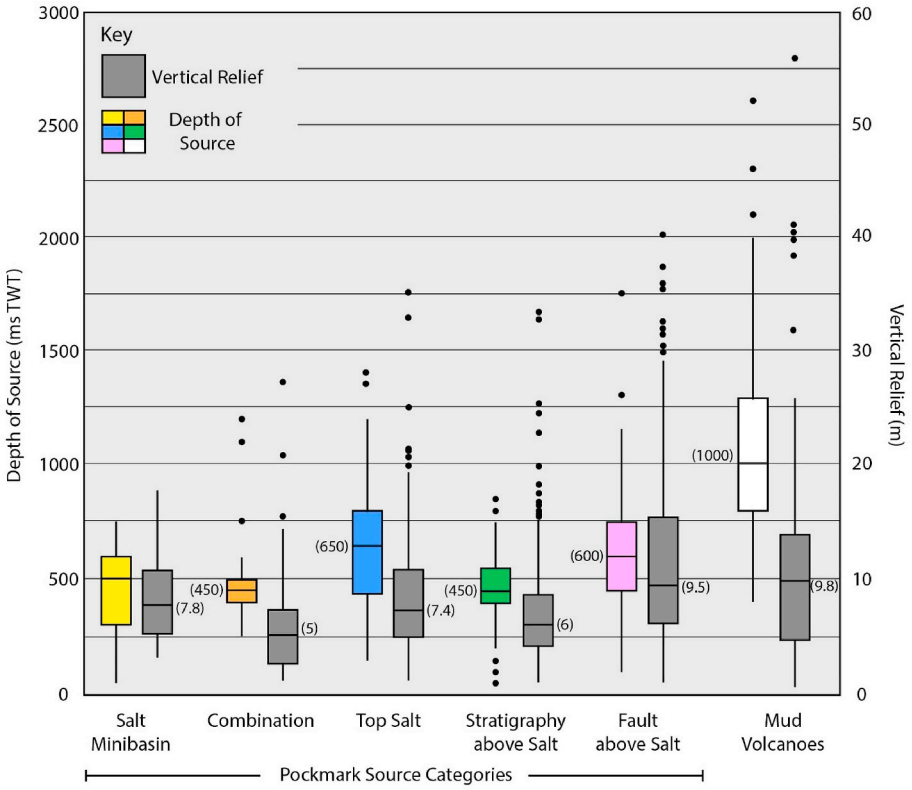

Fig. 19. Box plots showing the ranges of source depths (coloured boxes) and vertical relief (grey boxes) – negative for the pockmarks, positive for the mud volcanoes – across the different source categories. Graph shows generally similar sizes of the fluid flow features, whilst source depth is on average much deeper for the mud volcanoes compared with the pockmarks. Median values are labelled on the graph. Colours correspond to the different source categories labelled in the x-axis and match those in Figs. 12 and 21. (For interpretation of the references to colour in this figure legend, the reader is referred to the Web version of this article.)

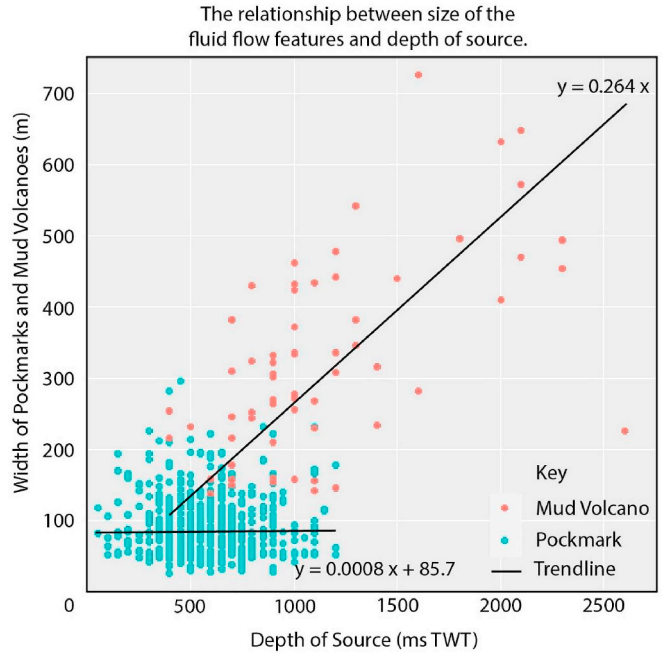

Fig. 20. Scatter graph of the width of pockmarks (blue) and mud volcanoes (red) plotted against source depth. A general positive trend is seen for the mud volcanoes, whilst no trend is evident for the pockmarks. The pockmarks are generally small and sourced in shallow strata, whilst mud volcanoes are larger and sourced from deeper parts of the salt minibasins. (For interpretation of the references to colour in this figure legend, the reader is referred to the Web version of this article.)

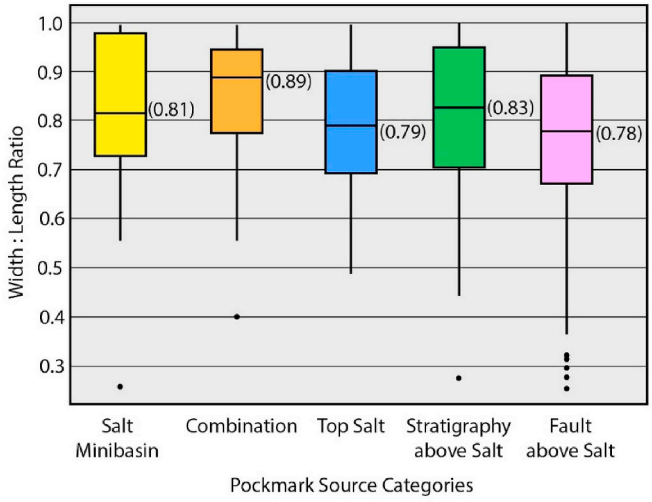

Fig. 21. Box plot showing the width:length ratios of the pockmarks across the different source categories. Lower w:l ratios correspond to greater eccentricity values. Most of the values lie between 0.7 and 1.0, whilst pockmarks associated with faults have slightly lower w:l ratios. Median values are labelled.

contrast, pockmarks reflect a shallow plumbing system. Despite their relative smaller size compared with the mud volcanoes, these are still large pockmarks compared to those mapped in other basins (Table 2), and represent significant volumes of shallow fluid escape to the sea floor.

8.3. Implications for hydrocarbon storage and leakage risk in East Breaks

The high proportion of pockmarks associated with the salt diapirs suggests that primary fluid bypass features in the study area are the salt diapirs and overlying faults. The dynamic nature of the salt deforms the overlying sedimentary units by faulting, and these faults are utilised by fluids as effective flow pathways from the top salt horizon to the sea floor. It is likely that large volumes of hydrocarbons have already leaked to the sea floor during the Cenozoic. The base of salt is also not imaged, indicating a very deep (> 8 s TWT) source of salt; hence, how

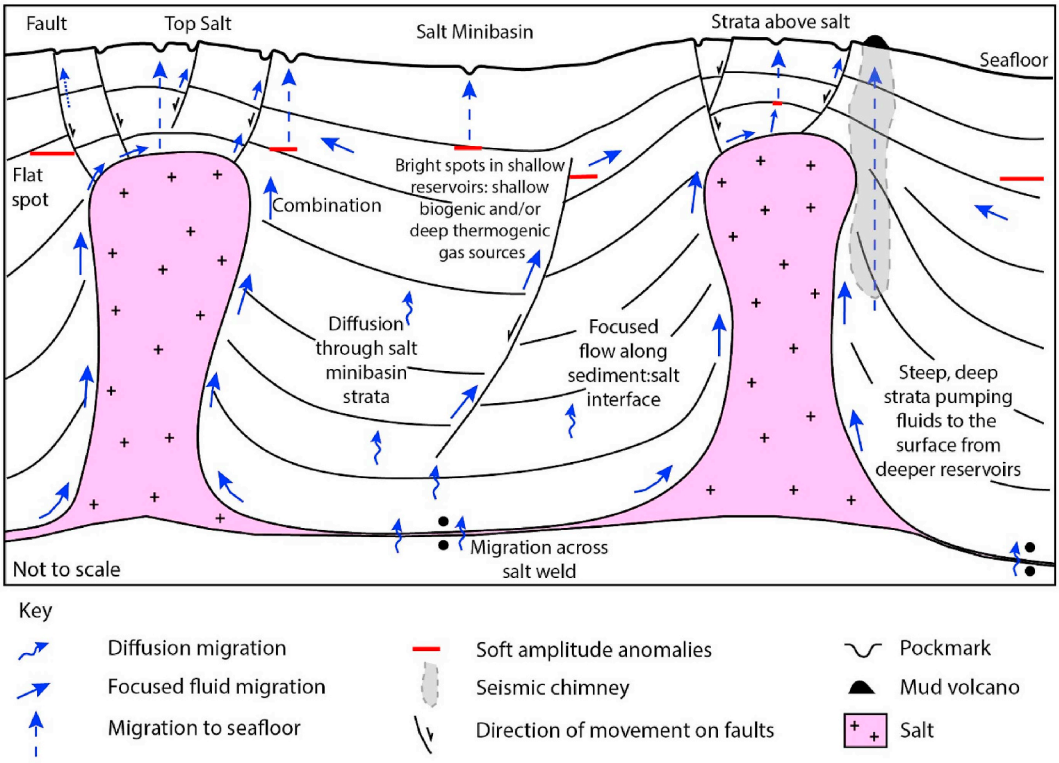

Fig. 22. Schematic summary of the plumbing system within the north-eastern region of East Breaks salt minibasin province, northern Gulf of Mexico. Blue arrows indicate the variety of migration pathways observed in the study area: across salt welds, through minibasin strata, along the sediment: salt interface, along faults, and vertically to the sea floor. Pockmarks are formed from shallow accumulations of gas, whilst seismic chimneys below mud volcanoes extend to the depths of minibasins, indicating relatively deeper sources. (For interpretation of the references to colour in this figure legend, the reader is referred to the Web version of this article.)

much more can the salt diapirs grow towards the surface? Weijermars et al. (2014) stated that salt may be moving up to 100 mm/yr in the Gulf of Mexico, revealing how mobile the salt is at present, posing further risks for drilling as exploration wells are deformed and fractured in such conditions.

Despite the small number of pockmarks in the minibasins, fluids migrated across the minibasin strata or along intra-minibasin faults to shallower units. Even though the high abundance of direct hydrocarbon indicators, and a relative absence of overlying pockmarks, allude to the potential of shallow hydrocarbon accumulations, it should be remembered that anomalies such as bright spots may arise as a result of gas saturations from only a few percent to complete gas saturation (Conn and Arthur, 1990; Judd and Hovland, 1992). They must be interpreted with caution. Even if these are not viable exploration accumulations, the presence of shallow gas presents another drilling hazard.

The varying quality of the seismic data made it difficult to interpret the underlying structures in several regions, increasing the risk in exploration. The source category 'combination' took this uncertainty into consideration. In some areas, the seismic inlines showed no salt, whilst cross-lines appeared to show underlying salt. This also alluded to the likelihood of dual-fluid sources into the same shallow reservoir: both from the deeper parts of the minibasins and from shallower, gently dipping stratigraphy.

There is clearly an active petroleum system in the study area, but how much has leaked already, and the location and depth of the main reservoirs, remain uncertain. The poor sub-salt data quality makes it difficult to predict where hydrocarbon accumulations may be underneath the flanks of the diapirs, if at all, but must not be ruled out, as several hydrocarbon fields in the world have been discovered in these settings. Examples include the Auger field in the Gulf of Mexico (Hearon et al., 2014) and the Merganser field in the Central North Sea (Charles and Ryzhikov, 2015). The surveys used in this study were acquired in 1991, therefore re-processing of the data, or newly acquired data, will be invaluable for imaging sub-salt, characterising the deeper structures to reveal possible hydrocarbon traps.

9. Conclusions

In this paper, three-dimensional seismic data, combined with semi-automated mapping methods in ArcGIS were used to analyse the morphology and distribution of 720 pockmarks and 62 mud volcanoes in the northern Gulf of Mexico. Mapping and characterising the pockmarks and mud volcanoes has allowed a detailed analysis and description of the key leakage pathways in the East Breaks area of the northern Gulf of Mexico, and our method is expected to be applicable to other areas in the Gulf of Mexico as well as other salt-rich basins around the world. The main conclusions of this work are as follows:

- Salt diapir edges and crestal faults are the dominant focused fluid flow pathways to the surface – supported by the evidence of 96% of the pockmarks being located above the salt diapirs.
- Diffusive fluid flow also occurred through the minibasin to shallower units, and focused fluid flow along intra-minibasin faults. Gas has accumulated in reservoirs consisting mainly of mass-transport complexes, from which fluid flow was also diverted sub-vertically towards the structural highs created by growing salt diapirs.
- Key seal bypass elements in this setting are supra-salt normal faults associated with extension above growing salt diapirs, vertical pipes and the resulting pockmarks on the sea floor. Hydrocarbon leakage is active at present day.
- Mud volcanoes are sourced from the deepest parts of the minibasins, whilst pockmarks represent shallow plumbing systems. Larger fluid flow features are associated with greater minibasin catchment area and dip.

- The semi-automated mapping method increases accuracy and reduces the time spent characterising shallow fluid-flow systems.

Declaration of competing interest

None.

Acknowledgements

The work in this study was conducted during a PhD study undertaken as part of the Natural Environment Research Council (NERC) Centre for Doctoral Training (CDT) in Oil and Gas. It is sponsored by Cardiff University and the British Geological Survey (BGS) via the British University Funding Initiative (BUFI) grant number GA/16S/007, whose support is gratefully acknowledged. The British Geological Survey (BGS) is thanked for provision of the BGS Seafloor Mapping Toolbox. We acknowledge the USGS for the seismic surveys. We also acknowledge Schlumberger (for Petrel®) and ESRI (for ArcGIS) for providing academic licences to Cardiff's 3D Seismic Lab. We acknowledge The Bureau of Ocean Energy Management (BOEM) for developing the Northern Gulf of Mexico Deepwater Bathymetry Grid and Seafloor Anomalies and making them publically available for use. We thank Dr Nathalia Mattos for her support with Petrel and we also thank the Editor-in-Chief, Dr Massimo Zecchin and the reviewers, Dallas Dunlap and Dr Mark Ireland for their constructive comments.

References

Andresen, K.J., Huuse, M., Clausen, O.R., 2008. Morphology and distribution of Oligocene and Miocene pockmarks in the Danish North Sea -implications for bottom current activity and fluid migration. Basin Res. 20 (3), 445–466. https://doi.org/10.1111/j.1365-2117.2008.00362.x.

Andresen, K.J., Huuse, M., Schødt, N.H., Clausen, L.F., Seidler, L., 2011. Hydrocarbon plumbing systems of salt minibasins offshore Angola revealed by three-dimensional seismic analysis. AAPG Bull. 95 (6), 1039–1065. https://doi.org/10.1306/12131010046.

Armentrout, J., 1999. Chapter 4: sedimentary Basin analysis. In: Treatise of Petroleum Geology/Handbook of Petroleum Geology: Exploring for Oil and Gas Traps, (pp. 4-1-4–123).

Badley, M.E., 1985. Practical Seismic Interpretation. IHRDC Press, Boston, MA: United States.

Beaubouef, R.T., Friedmann, S.J., 2000. High resolution seismic/sequence stratigraphic framework for the evolution of Pleistocene intra slope basins, western Gulf of Mexico: depositional models and reservoir analogs. In: Deep-Water Reservoirs of the World: 20th Annual, (September), pp. 40–60.

Bird, D.E., Burke, K., Hall, S.A., Casey, J.F., 2005. Gulf of Mexico tectonic history: hotspot tracks, crustal boundaries, and early salt distribution. AAPG Bull. 89 (3), 311–328. https://doi.org/10.1306/10280404026.

Boswell, R., Collett, T.S., Frye, M., Shedd, W., McConnell, D.R., Shelander, D., 2012. Subsurface gas hydrates in the northern Gulf of Mexico. Mar. Pet. Geol. 34 (1), 4–30. https://doi.org/10.1016/j.marpetgeo.2011.10.003.

Brown, A.R., 2011. Interpretation of Three-Dimensional Seismic Data. Society of Exploration Geophysicists and American Association of Petroleum Geologists.

Brown, M., 1990. The nature and hydrogeologic significance of mud diapirs and diatremes for accretionary systems. J. Geophys. Res. 95, 8969–8982.

Cartwright, J., Santamarina, C., 2015. Seismic characteristics of fluid escape pipes in sedimentary basins: implications for pipe genesis. Mar. Pet. Geol. https://doi.org/10.1016/j.marpetgeo.2015.03.023.

Charles, R., Ryzhikov, K., 2015. Merganser Field: Managing Subsurface Uncertainty during the Development of a Salt Diapir Field in the UK Central North Sea. Geological Society, London, pp. 403 Special Publications.

Chen, J., Song, H., Guan, Y., Yang, S., Pinheiro, L.M., Bai, Y., et al., 2015. Morphologies, classification and genesis of pockmarks, mud volcanoes and associated fluid escape features in the northern Zhongjiannan Basin, South China Sea. Deep-Sea Res. Part II Top. Stud. Oceanogr. 122, 106–117. https://doi.org/10.1016/j.dsr2.2015.11.007.

Clarke, P.J., Evans, F.C., 1954. Distance to nearest neighbor as a measure of spatial relationships in populations stable. Ecology 35 (4), 445–453.

Conn, P., Arthur, J., 1990. In: Ardus, D.A., Green, C.D. (Eds.), Safety in Offshore Drilling: the Role of Shallow Gas Surveys. Kluwer Academic Publishers, Dordrecht.

Dow, W.G., Yukler, M.A., Senftle, J.T., Kennicutt, M.C., Armentrout, J., 1990. Miocene oil source beds in the East Breaks basin, Flex-Trend, offshore Texas. In: Gulf Coast Section SEPM 9th Annual Research Conference, pp. 139–150.

Feng, J., 1995. Post Mid-cretaceous Seismic Stratigraphy and Depositional History, Deep Gulf of Mexico. University of Texas at Austin, Austin, Texas.

Gafeira, J., Long, D., Diaz-Doce, D., 2012. Semi-automated characterisation of seabed pockmarks in the Central North sea. Near Surf. Geophys. 10 (4), 303–314.

Gafeira, Joana, Dolan, M., Monteys, X., 2018. Geomorphometric characterization of pockmarks by using a GIS-based semi-automated Toolbox. Geosciences 8 (5), 154. https://doi.org/10.3390/geosciences8050154.

Galloway, W.E., 1989. Genetic stratigraphic sequences in basin analysis II: application to northwest Gulf of Mexico Cenozoic basin. Am. Assoc. Pet. Geol. Bull. 73 (2), 143–154. https://doi.org/10.1306/703C9AFA-1707-11D7-8645000102C1865D.

Galloway, W.E., Ganey-Curry, P.E., Li, X., Buffler, R.T., 2000. Cenozoic depositional history of the Gulf of Mexico basin. AAPG Bull. 84 (11), 1743–1774.

Galloway, William E., 2008. Chapter 15 depositional evolution of the Gulf of Mexico sedimentary basin. Sedimentary Basins of the World, vol. 5 Elsevier.

Gay, A., Lopez, M., Cochonat, P., Sultan, N., Cauquil, E., Brigaud, F., 2003. Sinuous pockmark belt as indicator of a shallow buried turbiditic channel on the lower slope of the Congo basin, West African margin. Subsurf. Sediment. Mobil. 216 (1), 173–190. https://doi.org/10.1144/gsl.sp.2003.216.01.12.

Geldof, J.-B., Gafeira, J., Contet, J., Marquet, S., 2014. GIS analysis of pockmarks from 3D seismic exploration surveys. In: Offshore Technology Conference, vol. 25088. pp. 1–10.

Gross, O.P., Hood, K.C., Wenger, L.M., Harrison, S.C., 1995. Seismic imaging and analysis of source and migration within an integrated hydrocarbon system study, northern Gulf of Mexico Basin. In: 1st Latin American Geophysical Conference, pp. 1–4.

Hackley, P.C., Ewing, T.E., 2010. Assessment of undiscovered conventional oil and gas resources, onshore Claiborne Group, United States part of the northern Gulf of Mexico Basin. AAPG Bull. 94 (10), 1607–1636.

Hasiotis, T., Papatheodorou, G., Kastanos, N., Ferentinos, G., 1996. A pockmark field in the Patras Guld (Greece) and its activation during the 14/7/93 seismic event. Mar. Geol. 130, 333–344.

Hearon, T.E., Rowan, M.G., Giles, K.A., Hart, W.H., 2014. Halokinetic Deformation Adjacent to the Deepwater Auger Diapir , Garden Banks 470 , Northern Gulf of Mexico : Testing the Applicability of an Outcrop-Based Model Using Subsurface Data. Interpretation, (November).

Ho, S., Hovland, M., Blouet, J., Wetzel, A., Imbert, P., 2018. Formation of linear planform chimneys controlled by preferential hydrocarbon leakage and anisotropic stresses in faulted fine-grained sediments , offshore Angola. Solid Earth 9, 1437–1468.

Hood, K.C., Wenger, L.M., Gross, O.P., Harrison, S.C., 2002. Hydrocarbon systems analysis of the northern Gulf of Mexico: delineation of hydrocarbon migration pathways using seeps and seismic imaging. Surf. Explor. Case Hist. Appl. Geochem. Magn. Rem. Sens. AAPG Stud. Geol. 48 (1), 25–40. Retrieved from. http://www.oilfield.searchanddiscovery.com/documents/hood/%5Cnpapers2://publication/uuid/F7DF6868-6F13-46AE-A48A-9DAA76E04C02.

Hovland, M., Judd, a.G., 1988. Seabed Pockmarks and Seepages — Impact on Geology, Biology and the Marine Environment. Graham & Trotman Ltd, London.

Hudec, M.R., Norton, I.O., Jackson, M.P.A., Peel, F.J., 2013. Jurassic evolution of the Gulf of Mexico salt basin. AAPG Bull. 97 (10), 1683–1710. https://doi.org/10.1306/04011312073.

Hutchinson, D., Ruppel, C., Roberts, H., Carney, R., Smith, M., 2011. Gas hydrates in the Gulf of Mexico. In: Holmes, C. (Ed.), Gulf of Mexico: its Origin, Waters, and Biota. Texas A&M University Press, pp. 247–275.

Jackson, M.P.A., Hudec, M.R., 2017. Salt Tectonics: Principles and Practice. Cambridge University Press.

Judd, A.G., Hovland, M., 1992. The evidence of shallow gas in marine sediments. Cont. Shelf Res. 12 (10), 1081–1095. https://doi.org/10.1016/0278-4343(92)90070-Z.

Judd, A.G., Hovland, M., 2007. Seabed Fluid Flow: the Impact on Geology, Biology and the Marine Environment, vol. 441 Campridge University Press, New York.

Kaiser, M.J., 2018. Review of Gulf of Mexico well activity highlights decline. Offshore Mag. (9), 2017–2019.

King, L.H., MacLean, B., 1970. Pockmarks on the Scotian Shelf. Bulletin of the Geological Society of America.

Kramer, K.V., Shedd, W.W., 2017. A 1.4-Billion-Pixel Map of the Gulf of Mexico Seafloor.

Krijgsman, W., Hilgen, F.J., Raffi, I., Sierro, F.J., Wilson, D.S., 1999. Chronology , causes and progression of the Messinian salinity crisis. Nature 400 (August), 652–655.

Løseth, H., Wensaas, L., Arntsen, B., Hanken, N.M., Basire, C., Graue, K., 2011. 1000 M long gas blow-out pipes. Mar. Pet. Geol. 28 (5), 1040–1060. https://doi.org/10.1016/j.marpetgeo.2010.10.001.

Maia, A.R., Cartwright, J., Andersen, E., 2016. Shallow plumbing systems inferred from spatial analysis of pockmark arrays. Mar. Pet. Geol. 77, 865–881. https://doi.org/10.1016/j.marpetgeo.2016.07.029.

Marfurt, K.J., Alves, T.M., 2014. Pitfalls and limitations in seismic attribute interpretation of tectonic features. Interpretation 3 (1), SB5–SB15. https://doi.org/10.1190/INT-2014-0122.1. Retrieved from.

Mazzini, A., 2009. Mud volcanism : processes and implications. Mar. Pet. Geol. 26 (9), 1677–1680. https://doi.org/10.1016/j.marpetgeo.2009.05.003.

McBride, B.C., Rowan, M.G., Weimer, P., 1998. The evolution of allochthonous salt systems, northern Green Canyon and Ewing Bank (offshore Louisiana), northern Gulf of Mexico. AAPG Bull. 82 (5 B), 1013–1036. https://doi.org/10.1306/1D9BC9FD-172D-11D7-8645000102C1865D.

Mello, U.T., Karner, G.D., 1996. Development of sediment overpressure and its effect on thermal maturation: application to the Gulf of Mexico basin. AAPG Bull. 80 (9), 1367–1396. https://doi.org/10.1306/64ED9A42-1724-11D7-8645000102C1865D.

Milkov, A.V., 2000. Worldwide distribution of submarine mud volcanoes and associated gas hydrates. 167, 29–42.

Moss, J.L., Cartwright, J., Cartwright, A., Moore, R., 2012. The spatial pattern and drainage cell characteristics of a pockmark field, Nile Deep Sea Fan. Mar. Pet. Geol. 35 (1), 321–336. https://doi.org/10.1016/j.marpetgeo.2012.02.019.

Pietzsch, R., Oliveira, D.M., Tedeschi, L.R., Neto, J.V.Q., Figueiredo, M.F., Vazquez, J.C., Schi, R., 2018. Palaeohydrology of the Lower Cretaceous pre-salt lacustrine system , from rift to post-rift phase , Santos Basin , Brazil. Palaeogeogr. Palaeoclimatol. Palaeoecol. 507 (June), 60–80. https://doi.org/10.1016/j.palaeo.2018.06.043.

Prather, B.E., Booth, J.R., Steffens, G.S., Craig, P.A., 1998. Classification, lithologic calibration, and stratigraphic succession of seismic facies of intraslope basins, deep-water Gulf of Mexico. AAPG Bull. 82 (5 A), 701–728. https://doi.org/10.1306/1D9BC5D9-172D-11D7-8645000102C1865D.

Rollet, N., Logan, G.A., Ryan, G., Judd, A.G., Totterdell, J.M., Glenn, K., et al., 2009. Shallow gas and fluid migration in the northern Arafura Sea (offshore Northern Australia). Mar. Pet. Geol. 26 (1), 129–147. https://doi.org/10.1016/j.marpetgeo.2007.07.010.

Rowan, M.G., Jackson, M.P.A., Trudgill, B.D., 1999. Salt related fault families and falt welds in the northern Gulf of Mexico. AAPG Bull. 83 (9), 1454–1484. https://doi.org/10.1306/E4FD41E3-1732-11D7-8645000102C1865D.

Salvador, A., 1987. Late Triassic-Jurassic paleogeography and origin of Gulf of Mexico. AAPG Bull. 71 (4), 419–451. https://doi.org/10.1306/2F917F19-16CE-11D7-8645000102C1865D.

Speight, J.G., 2011. Chapter 2: sources of hydrocarbons. In: Handbook of Industrial Hydrocarbon Processes. Elsevier Inc, pp. 43–83.

Tasianas, A., Bünz, S., Bellwald, B., Hammer, Ø., Planke, S., Lebedeva-Ivanova, N., Krassakis, P., 2018. High-resolution 3D seismic study of pockmarks and shallow fluid flow systems at the Snøhvit hydrocarbon field in the SW Barents Sea. Marine Geol. 403, 247–261.

Thompson, K.F., Kennicutt, M., Brooks II, J., 1990. Classification of offshore Gulf of Mexico oils and gas condensates. AAPG Bull. 74, 187–198.

Watts, A.B., 1982. Tectonic subsidence, flexure and global changes of sea level. Nature 297 (5866), 469–474. https://doi.org/10.1038/297469a0.

Weijermars, R., Jackson, M.P.A., Dooley, T.P., 2014. Quantifying drag on wellbore casings in moving salt sheets. Geophys. J. Int. 198 (2), 965–977. https://doi.org/10.1093/gji/ggu174.

Xia, C., Wilkinson, M., 2017. The geological risks of exploring for a CO 2 storage reservoir. Int. J. Greenh. Gas Control 63 (July), 272–280. https://doi.org/10.1016/j.ijggc.2017.05.016.